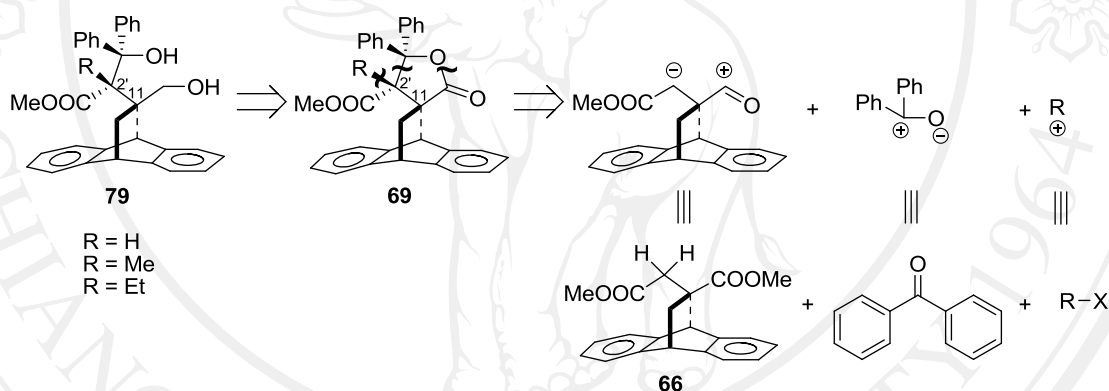


CHAPTER 3

RESULTS AND DISCUSSION

In this research, we focused on synthesizing the TADDOL–anthracene catalysts **79** in optically active pure forms from enantiomeric dimethyl itaconate–anthracene adducts (+)-(11*S*)-**66** and (–)-(11*R*)-**66**. In order to achieve the synthesis of the catalysts, it could be synthesized as following the retrosynthesis below (Scheme 12).



Scheme 12 Retrosynthesis of TADDOL–anthracene catalysts **79**.

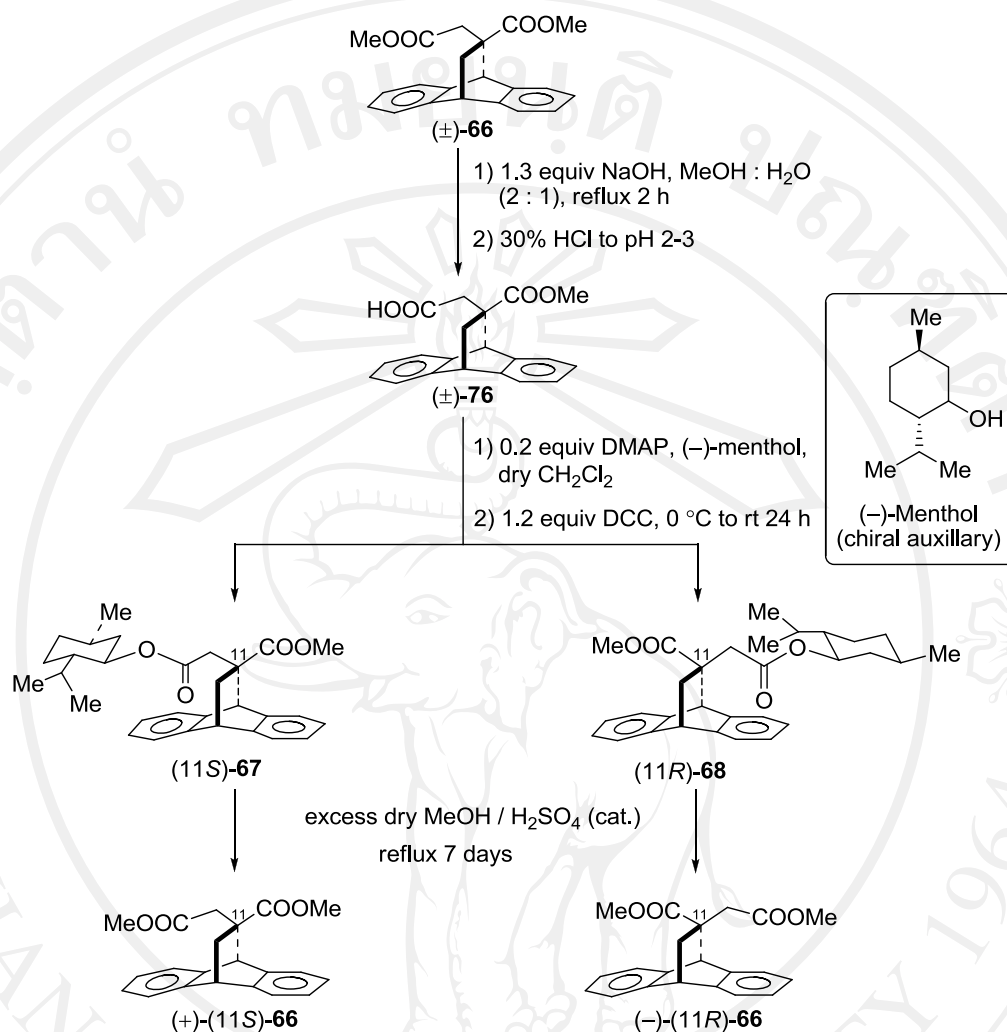
As can be seen from Scheme 12, we studied the synthesis of the catalysts by using the dimethyl itaconate–anthracene adduct and benzophenone as model reaction.

3.1 Preparation of optically active dimethyl itaconate–anthracene adducts (+)-(11*S*)-**66** and (–)-(11*R*)-**66**

To synthesize the spiro–lactone compounds in enantiomerically pure forms, the synthesis was started by resolution of the racemic dimethyl itaconate–anthracene adduct (\pm)-**66** by hydrolysis of racemic compound (\pm)-**66** with 1.2 equiv NaOH in

MeOH : H₂O (2 : 1) for 1 hour then obtained the monoacid adduct (±)-**76** in 58% yield. Afterward, resolution of racemic compound to diastereomeric compounds, the monoacid (±)-**76** was treated with DMAP (0.2 equiv), DCC (1.2 equiv) and (-)-menthol (1.2 equiv) as chiral auxiliary in dry CH₂Cl₂ at 0°C to room temperature for overnight. The crude product was recrystallized to provide two diastereoisomers, (-)-(11*S*)-**67** (13.1323 g, 43% yield), $[\alpha]_D^{34.3} = -144.93^\circ$ ($c = 0.109$, CHCl₃) and (-)-(11*R*)-**68** (13.1729 g, 43% yield), $[\alpha]_D^{29.2} = -82.23^\circ$ ($c = 0.231$, CHCl₃)

Both of enantiomeric dimethyl itaconate–anthracene adducts (+)-(11*S*)-**66** and (-)-(11*R*)-**66** were obtained by transmethylation of the two monomenthyl adducts, (-)-(11*S*)-**67** and (-)-(11*R*)-**68**, in an anhydrous methanol with sulfuric acid as catalyst, followed by recrystallization in CH₂Cl₂/hexane to give both optically active adducts (+)-(11*S*)-**66** in 83% yield, $[\alpha]_D^{27.2} = +80.83^\circ$ ($c = 0.141$, CHCl₃) and (-)-(11*R*)-**66** in 80%, ($[\alpha]_{589}^{30.6} = -83.62^\circ$ ($c = 0.110$, CHCl₃)).

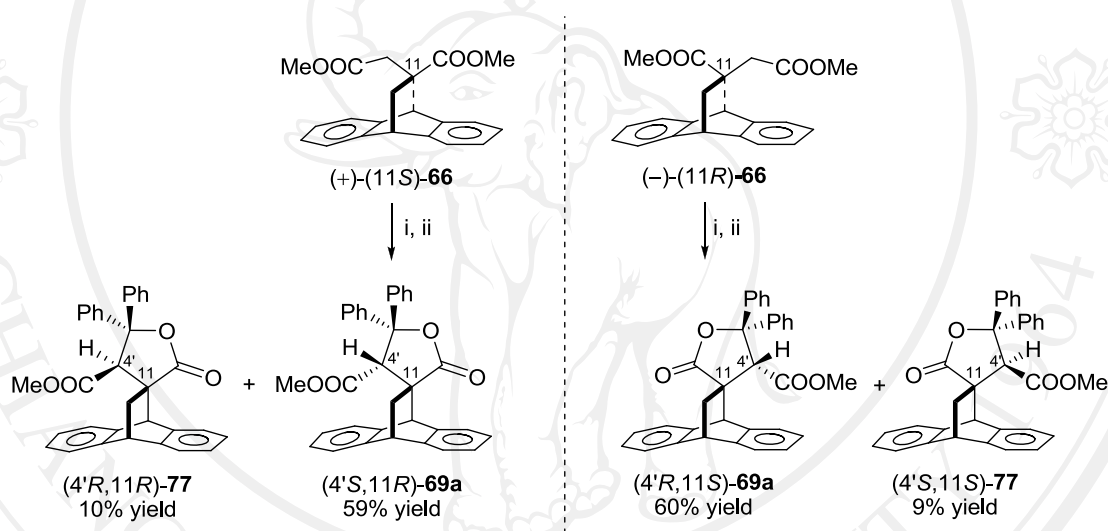


Scheme 13 Resolution of dimethyl itaconate–anthracene adducts (+)-(11S)-66 and (-)-(11R)-66.

3.2 Syntheses both of enantiomerically pure forms tetrahydro-4'-carbomethoxy-5'-diphenyl-2'-hydroxy-2'-phenyl-furanone-3'-spiro-11-9,10-dihydro-9,10-ethanoanthracenes [(4'S,11R)-69a, (4'R,11R)-77, (4'R,11S)-69b and (4'S,11S)-77]

The spiro-lactone compounds **69a** and **77** were synthesized by using optically active dimethyl itaconate–anthracene adducts (+)-(11S)-66 and (-)-(11R)-66 reacted

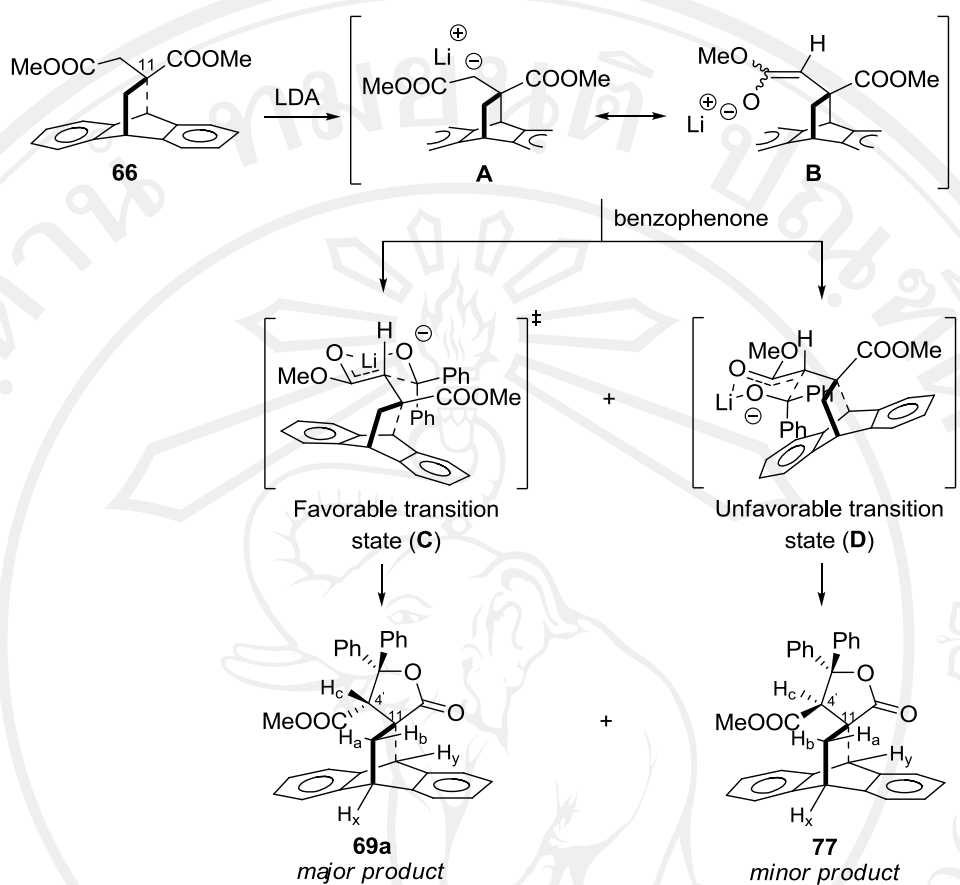
with lithium diisopropylamide (LDA, 1.2 equiv) in THF at 0 °C for 2 hours. The reaction was completed by enolate anions **A** and **B** (Scheme 15) reacted with benzophenone at -78 °C to room temperature for overnight followed by 10 % hydrochloric acid work up. The crude product was purified by flash column chromatography on silica gel with elution of EtOAc : CH₂Cl₂ : hexane = 0.5 : 1 : 8.5 afforded two diastereomeric spiro-lactone adducts, compound **69a** as major product and compound **77** as minor product as shown in Scheme 14.



Scheme 14 Synthesis both of enantiomeric spiro-lactone adducts **69a** and **77**.

Reagents and conditions: (i) 1.2 equiv LDA, THF, -78 °C to 0 °C, 1 h, (ii) 1.2 equiv benzophenone, 0°C to rt, overnight.

To clarify the orientation of H_c at α -position, the chair-like transition state which had the steric repulsion between phenyl group and the anthracene ring was utilized to explain *via* models **C** and **D** as shown in Scheme 15. Considering the stable transition state **C** which had less steric repulsion than **D**, the transition state **C** led to the major product **69a** while the transition state **D** led to the minor product **77**.



Scheme 15 Schematic represents the proposed mechanism of tandem aldol-lactonization of the spiro-lactone adducts.

The relative stereochemistries of the two spiro-lactones were determined by ^1H NMR and NOE experiment (Figure 14, 16 and Table 28). In case of major spiro-lactone compound **69a**, the signal of proton H_c appeared as singlet at δ 3.40 ppm, proton H_y appeared as singlet at δ 4.70 ppm and proton H_a appeared as doublet of doublets at δ 1.58 ppm ($J = 13.1, 2.6$ Hz). Consequently, NOE correlation showed that H_c enhanced with proton H_a but no NOE effect with H_y . Hence, it indicated that the orientation of proton H_c was on the upper face as proton H_a . Furthermore, the structures of both enantiomeric major spiro-lactone ($4'S,11R$)-**69a** and ($4'R,11S$)-**69a**

could be confirmed by MM2 force field calculations for energy minimization from modeling program ChemBio3D Ultra 11.0 program as depicted in Figure 13.

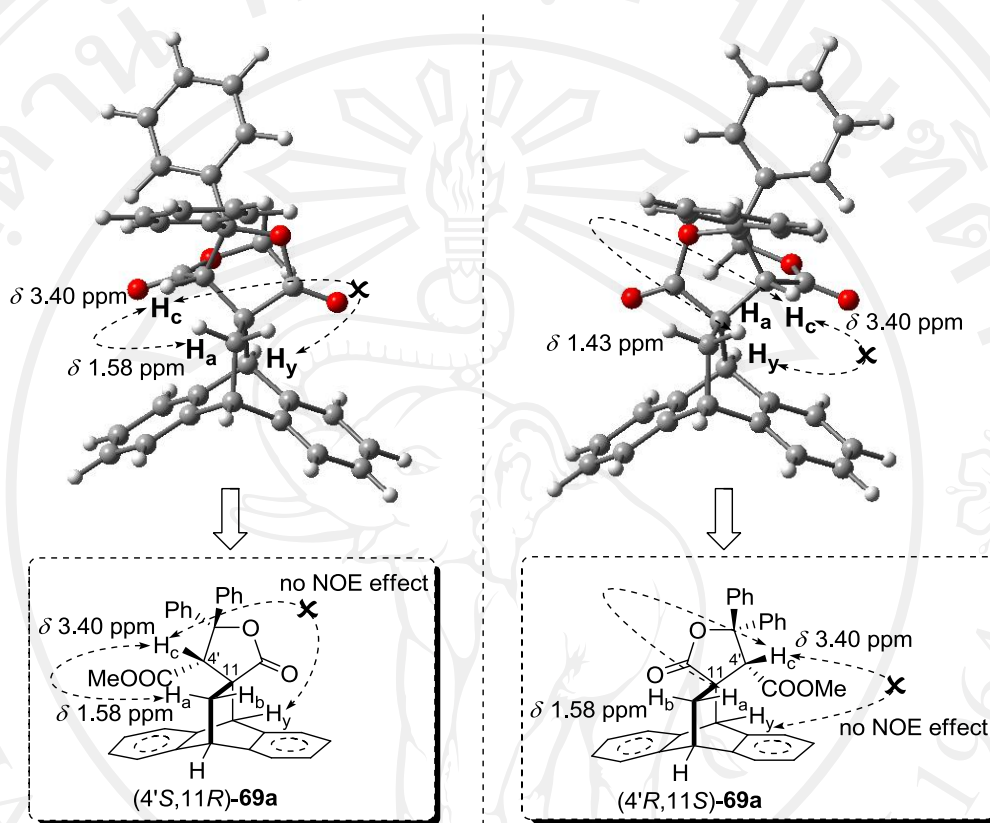


Figure 13 3D structural conformations of both forms of major spiro-lactone adducts ($4'S,11R$)-**69a** and ($4'R,11S$)-**69a** were generated by MM2 force field calculations for energy minimization from modeling program Chem3D Ultra 11.0 and GaussView 3.09 program with the observed NOE correlations (arrows)

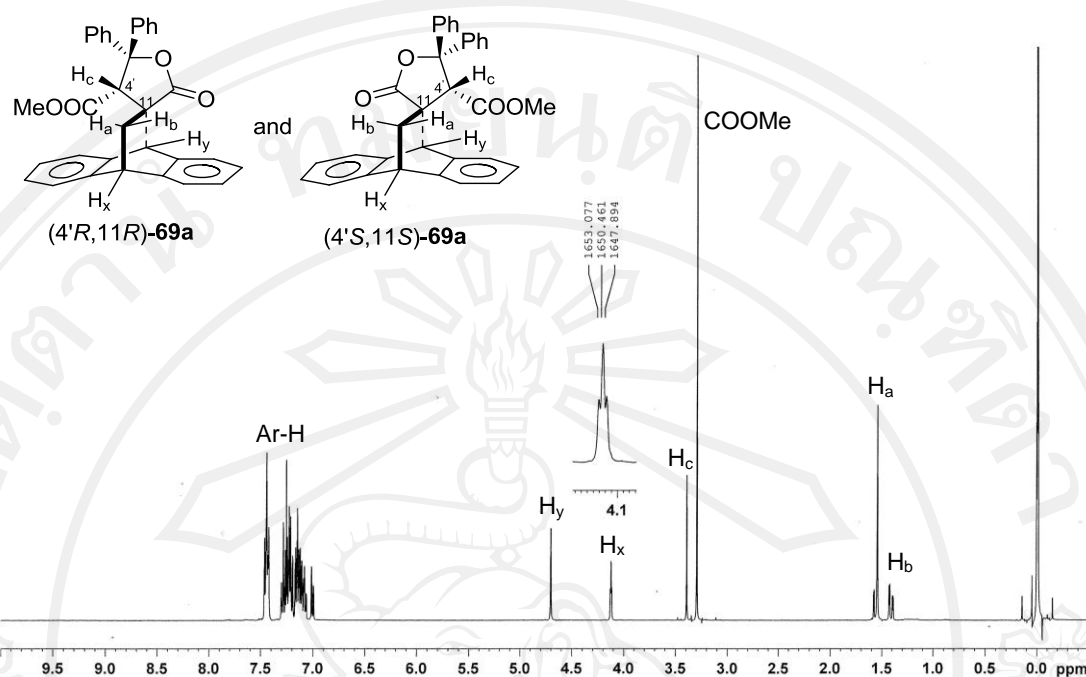


Figure 14 $^1\text{H-NMR}$ spectral data of major spiro-lactone adducts $(4'S,11R)$ -**69a** and $(4'R,11S)$ -**69a**

Besides, the minor spiro-lactone adducts $(4'R,11R)$ -**77** and $(4'S,11S)$ -**77**, the signal of proton H_c appeared as singlet at δ 3.72 ppm, proton H_y appeared as singlet at δ 3.92 ppm and proton H_a appeared as doublet of doublets at δ 2.43 ppm ($J = 13.2, 2.7$ Hz). In addition, NOE result showed that proton H_c could not enhance with proton H_a but enhanced with H_y . Thus, the orientation of proton H_c was on the lower face as proton H_y . The 3D structural and NOE correlation of both enantiomeric minor spiro-lactone adducts $(4'R,11R)$ -**77** and $(4'S,11S)$ -**77** was shown in Figure 15.

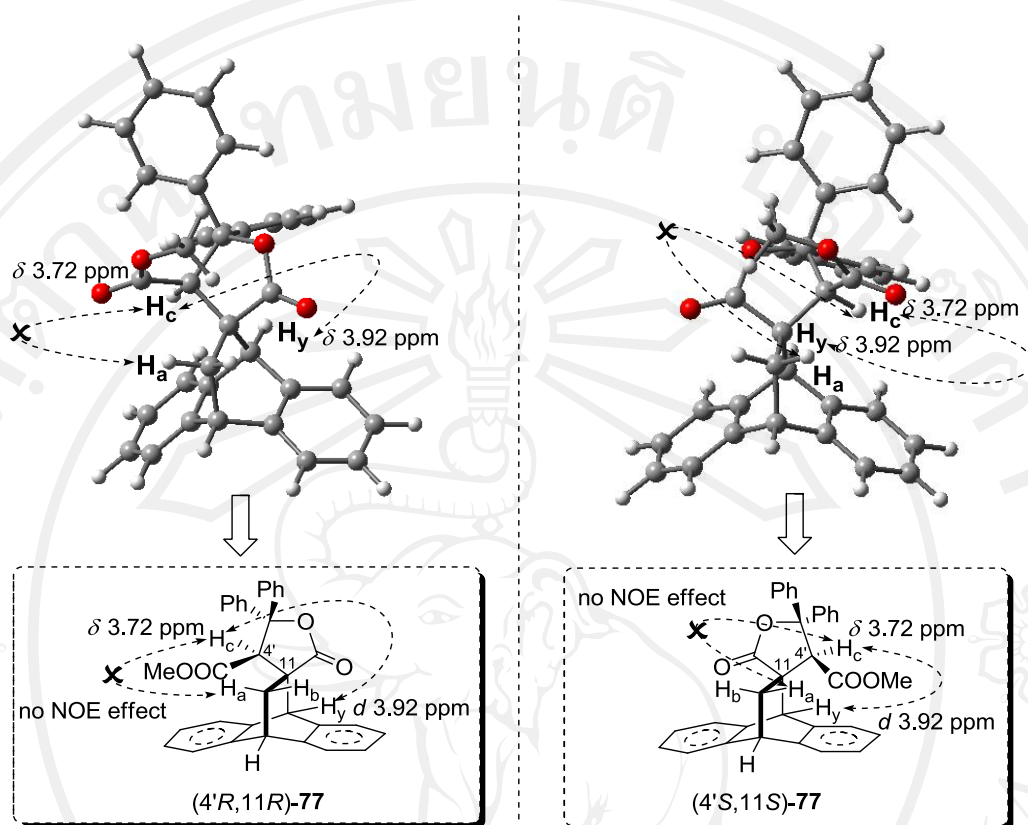


Figure 15 3D structural conformations of both forms of minor spiro-lactone adducts $(4'R,11R)$ -77 and $(4'S,11S)$ -77 were generated by MM2 force field calculations for energy minimization from modeling program Chem3D Ultra 11.0 and GaussView 3.09 program with the observed NOE correlations (arrows)

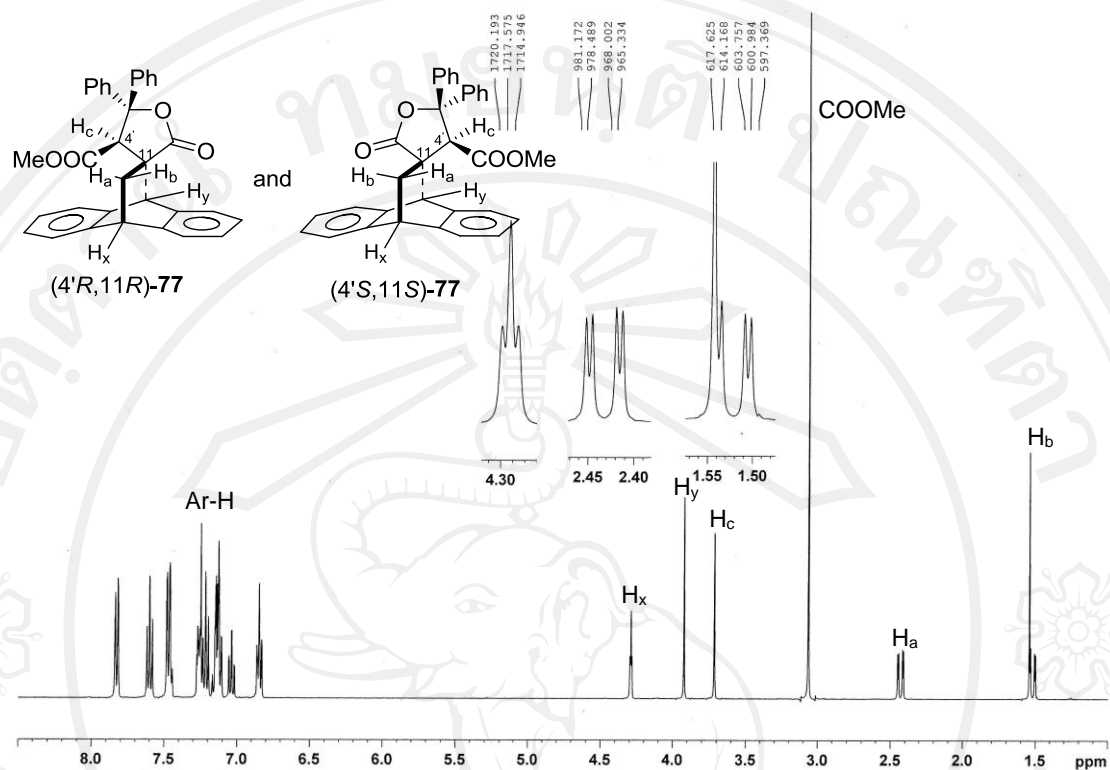


Figure 16 $^1\text{H-NMR}$ spectral data of minor spiro-lactone adducts ($4'R,11R$)-**77** and ($4'S,11S$)-**77**

Table 28 depicted the $^1\text{H-NMR}$ data of the major and minor spiro-lactone adducts.

Table 28 $^1\text{H-NMR}$ data of both enantiomeric major and minor spiro-lactone adducts **69a** and **77**

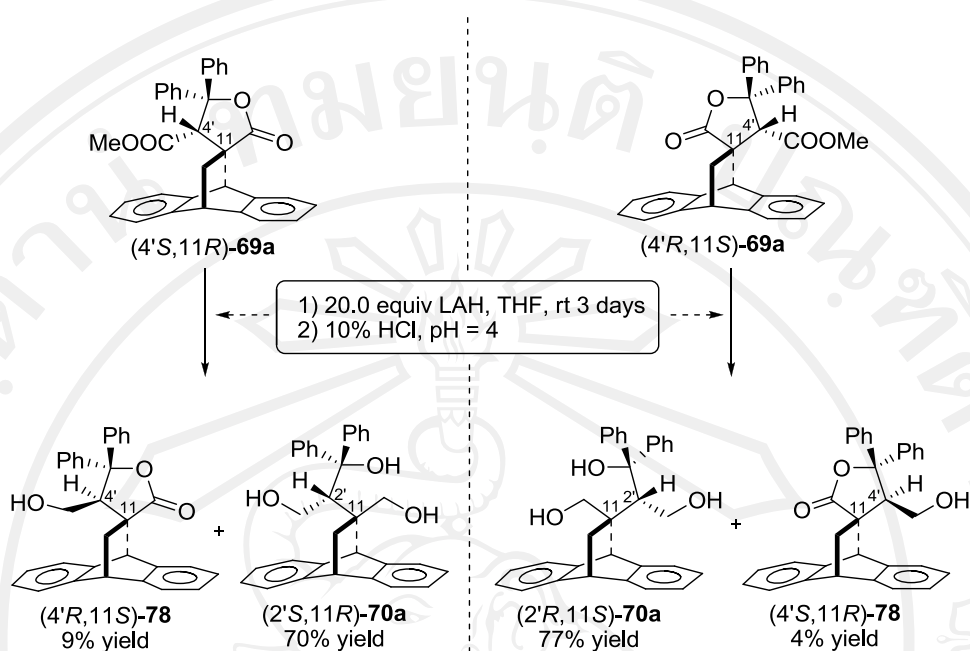
Compound	Physical property	m.p. ($^{\circ}\text{C}$)	Chemical shift (δ , ppm)
($4'S,11R$)- 69a and	White crystals	264.0–265.1	1.41, 1.58, 4.12 (<i>ABX</i> system ($J = 13.1$, 3.1, 2.6 Hz), 3H, H_a , H_b , H_x), 3.30 (<i>s</i> , 3H, COOCH_3 -7'), 3.40 (<i>s</i> , 1H, H_c), 4.70 (<i>s</i> , 1H, H_y), 7.00-7.48 (<i>m</i> , 18H, ArH-1, 2, 3, 4, 5, 6, 7, 8, 2'', 3'', 4'', 5'', 6'', 2''', 3''', 4'''),

Table 28 $^1\text{H-NMR}$ data of both enantiomeric major and minor spiro-lactone adducts **69a** and **77** (continued)

Compound	Physical property	m.p. (°C)	Chemical shift (δ , ppm)
(4' <i>R</i> ,11 <i>S</i>)- 69a			5''', 6''') (as shown in Figure 14)
(4' <i>R</i> ,11 <i>R</i>)- 77 and (4' <i>S</i> ,11 <i>S</i>)- 77	White crystals	263.4–265.2	1.52, 2.43, 4.29 (<i>ABX</i> system ($J = 13.2, 3.5, 2.7$ Hz), 3H, H_a, H_b, H_x), 3.07 (<i>s</i> , 3H, COOCH ₃ -7'), 3.72 (<i>s</i> , 1H, H_c), 3.92 (<i>s</i> , 1H, H_y), 6.84–7.84 (<i>m</i> , 18H, ArH-1, 2, 3, 4, 5, 6, 7, 8, 2'', 3'', 4'', 5'', 6'', 2''', 3''', 4''', 5''', 6''') (as shown in Figure 16)

3.3 Syntheses both forms of optically active 11-hydroxymethylene-11-(2'-(1',3'-dihydroxy-1',1'-diphenylpropyl))-9,10-dihydro-9,10-ethanoanthracene [(2'*S*,11*R*)-**70a** and (2'*R*,11*S*)-**70a**]

Both forms of the major spiro-lactone adducts (2'*S*,11*R*)-**69a** and (2'*R*,11*S*)-**69a** were reduced by an excess LAH in THF for 3 days quenched by acetone and followed by 10% hydrochloric acid solution at 0°C for pH = 4. The crude mixtures were purified by flash column chromatography (silica gel, EtOAc : hexane = 1 : 9 as eluent) and PLC (silica gel, EtOAc : hexane = 1 : 9 as developing solvent) to obtain triol TADDOL-anthracene adduct **70a** as major product and reduced compound **78** as minor product (Scheme 16).



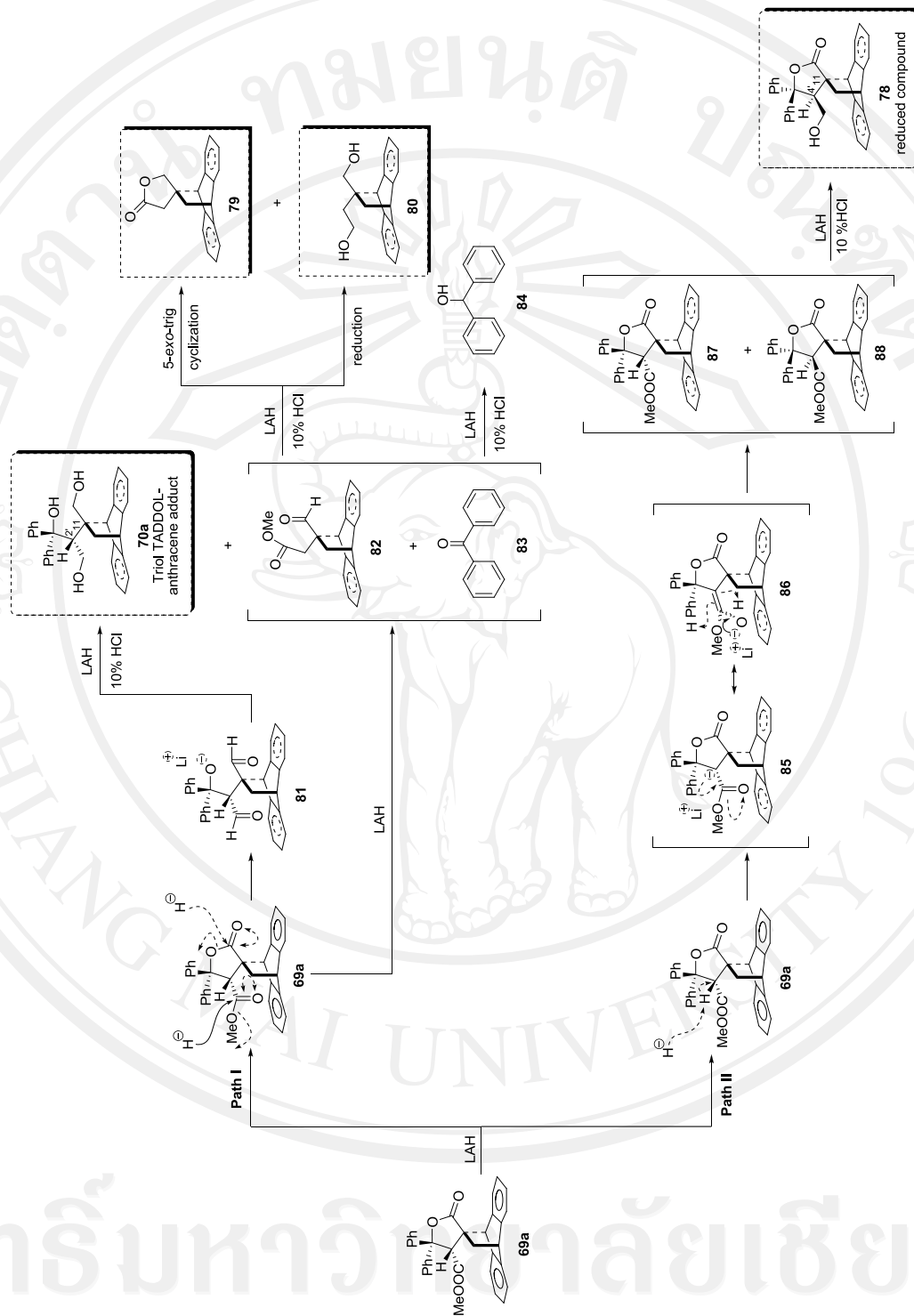
Scheme 16 Reduction of the major spiro-lactone adducts (4'S,11R)-**69a** and (4'R,11S)-**69a** by an excess lithium aluminium hydride.

The reduction of the major spiro-lactone adducts (4'S,11R)-**69a** and (4'R,11S)-**69a** with an excess LAH afforded two main compounds which were triol TADDOL-anthracene adducts (2'S,11R)-**70a** and (2'R,11S)-**70a** as major products and reduced compounds (4'R,11S)-**78** and (4'S,11R)-**78** as minor products. Furthermore, compound **79** and compound **80** were obtained as by-products. The mechanism of reducing the major spiro-lactone adduct could be proposed in two pathways; hydride from LAH acted as reducing agent (path I) and base (path II) as shown in Scheme 17.

In path I, hydride acted as reducing agent which reduced the spiro-lactone adduct **69a** and then ring opening afforded triol TADDOL-anthracene adduct **70a** as major product *via* intermediate **81**. Furthermore, intermediate **81** could be reduced

that effected to break into two portions which were dicarbonyl **82** and benzophenone **83**, respectively. The dicarbonyl **82** was ring closure *via* 5-*exo*-trig cyclization to give compound **79** and reduced to 1,4-diols compound **80** as by-products.

Besides, in path II, hydride performed as base to abstract α -hydrogen generated enolate anions (**85** and **86**) obtained the lactone in two forms which had α -proton on upper and lower face (**87** and **88**), respectively. However, the reduced compound **78** was only obtained from the lower face α -proton **88**.



Scheme 17 Proposed mechanism of reducing spiro-lactone by LAH.

The relative stereochemistries of all compounds were elucidated by ^1H NMR (Figure 18, 20, 21, 22 and Table 29). In case of triol TADDOL–anthracene adducts ($2'S,11R$)-**70a** and ($2'R,11S$)-**70a**, the signal of proton H_c appeared at 2.25 ppm as singlet, proton H_y shown the signal at 4.69 ppm as singlet and proton H_a at 1.36 ppm as doublet of doublets ($J = 13.5$ and 2.6 Hz). The proton H_c showed the greatest interaction with H_a more than H_y . Thus, the NOE correlation indicated that the proton H_c oriented on the upper face as H_a . Besides, the two protons at methylene C-3' showed the signals at 3.97 and 4.51 ppm as doublet with coupling constant, $J = 12.9$ Hz which were *trans*- configuration. Moreover, the connectivity at C-1', C-2', C-2'' and positions of hydroxyl groups were confirmed by HMBC, HMQC and COSY correlations. Figure 18 showed ^1H NMR of triol TADDOL–anthracene adducts ($2'S,11R$)-**70a** and ($2'R,11S$)-**70a**. Furthermore, the structures of both enantiomeric triol TADDOL–anthracene adducts ($2'S,11R$)-**70a** and ($2'R,11S$)-**70a** could be confirmed by MM2 force field calculations for energy minimization from modeling program ChemBio3D Ultra 11.0 program as depicted in Figure 17.

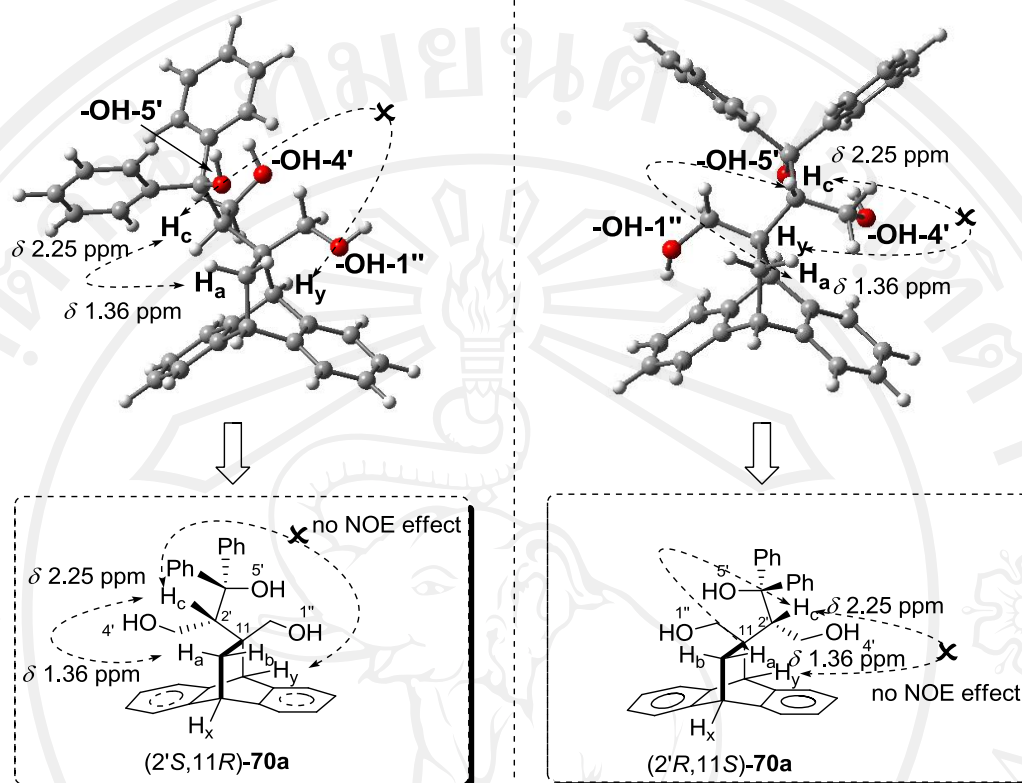


Figure 17 3D structural conformations of triol TADDOL–anthracene adducts (*2'S,11R*)-**70a** and (*2'R,11S*)-**70a** were generated by MM2 force field calculations for energy minimization from modeling program Chem3D Ultra 11.0 and GaussView 3.09 program with the observed NOE correlations (arrows)

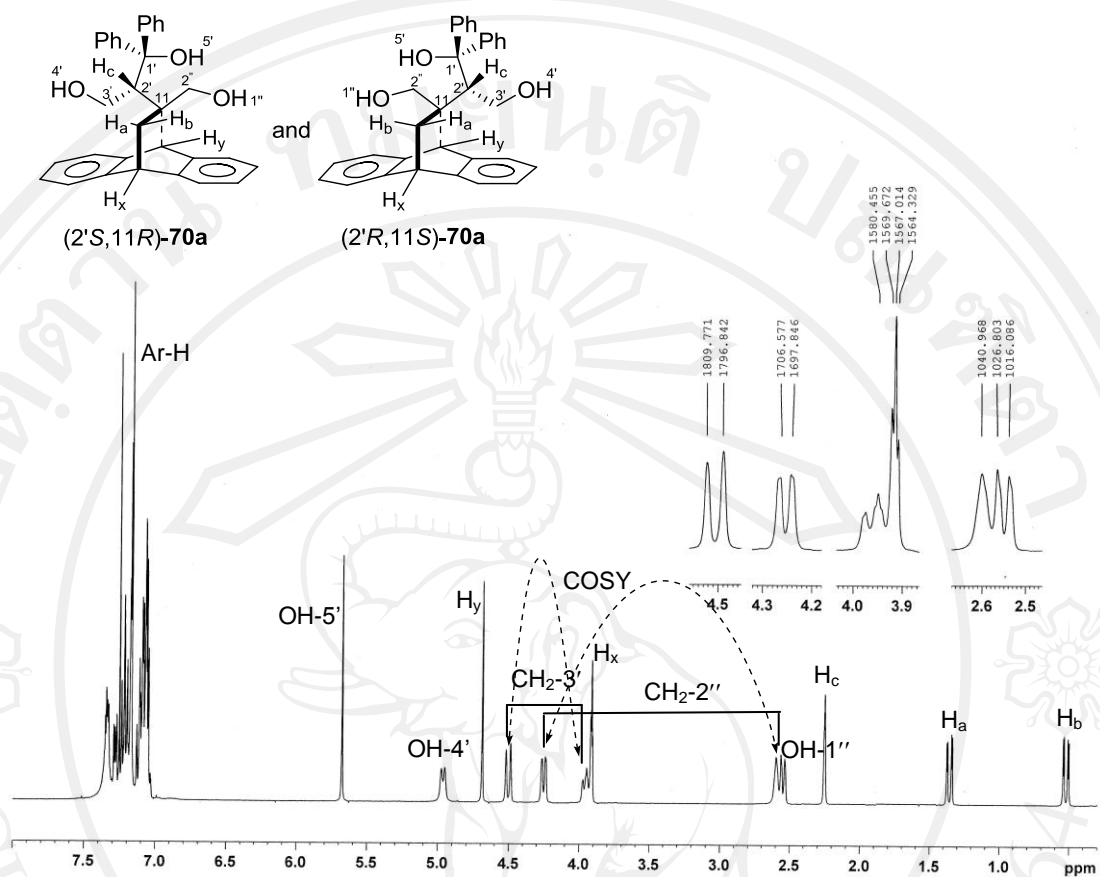


Figure 18 ¹H-NMR spectral data of triol TADDOL-anthracene adducts (2'S,11R)-70a and (2'R,11S)-70a (Dash arrows were COSY correlation)

To examine the orientation at proton H_c of minor products, reduced compounds (4'R,11S)-78 and (4'S,11R)-78, the signal of proton H_c appeared at 3.41 ppm as singlet, proton H_y showed the signal at 4.05 ppm as singlet and proton H_a at 2.18 ppm as doublet of doublets ($J = 13.4$ and 2.4 Hz). NOE correlation only showed the interaction between proton H_c and proton H_y. Hence, the proton H_c oriented on the lower face as H_y. Besides, the two protons at methylene C-6', proton H_c and H_d, showed the signals at 3.67 and 3.84 ppm as doublet with coupling constant, $J = 8.7$ Hz as shown in Figure 20. In addition, HMBC illustrated the correlation between hydroxyl group at C-6' and quaternary C-5' protons. Moreover, the correlation at

methylene C-6' and hydroxyl group were confirmed by HMBC, COSY and NOE correlation, respectively. The structures of reduced compounds (*4'R,11S*)-**78** and (*4'S,11R*)-**78** could be confirmed by MM2 force field calculations for energy minimization from modeling program ChemBio3D Ultra 11.0 program as depicted in Figure 19.

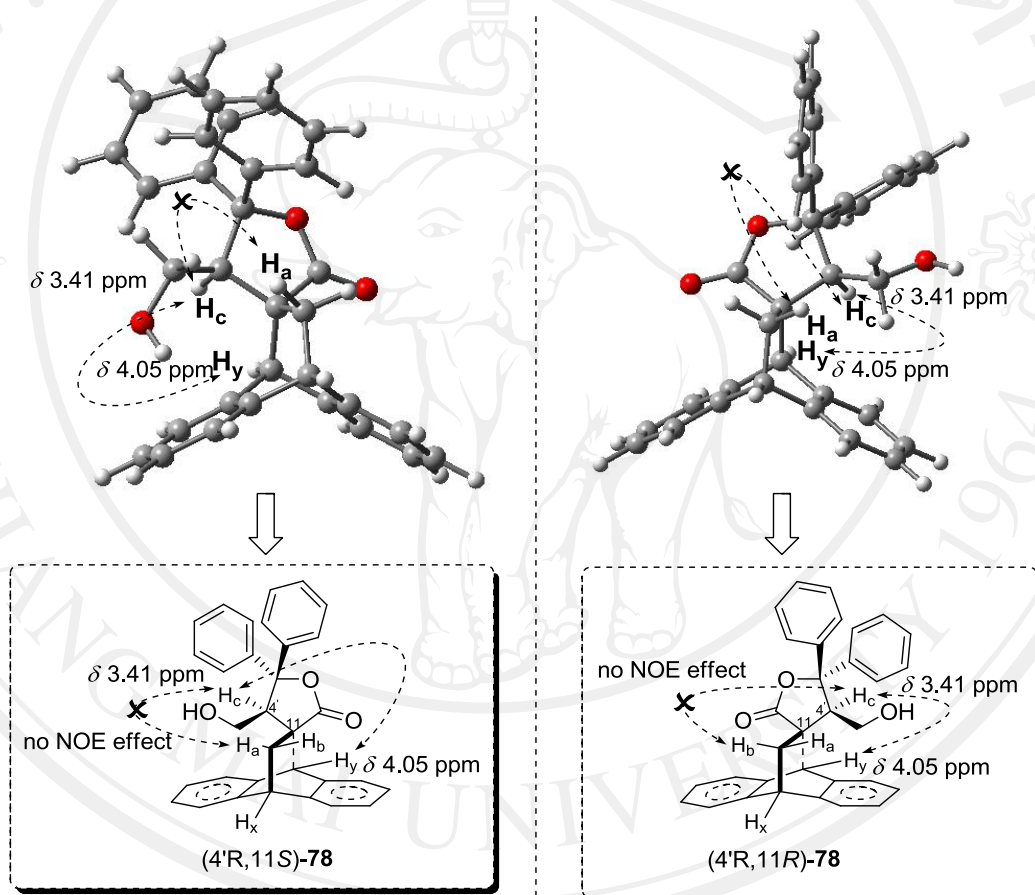


Figure 19 3D structural conformations of reduced compounds (*4'R,11S*)-**78** and (*4'S,11R*)-**78** were generated by MM2 force field calculations for energy minimization from modeling program Chem3D Ultra 11.0 and GaussView 3.09 program with the observed NOE correlations (arrows)

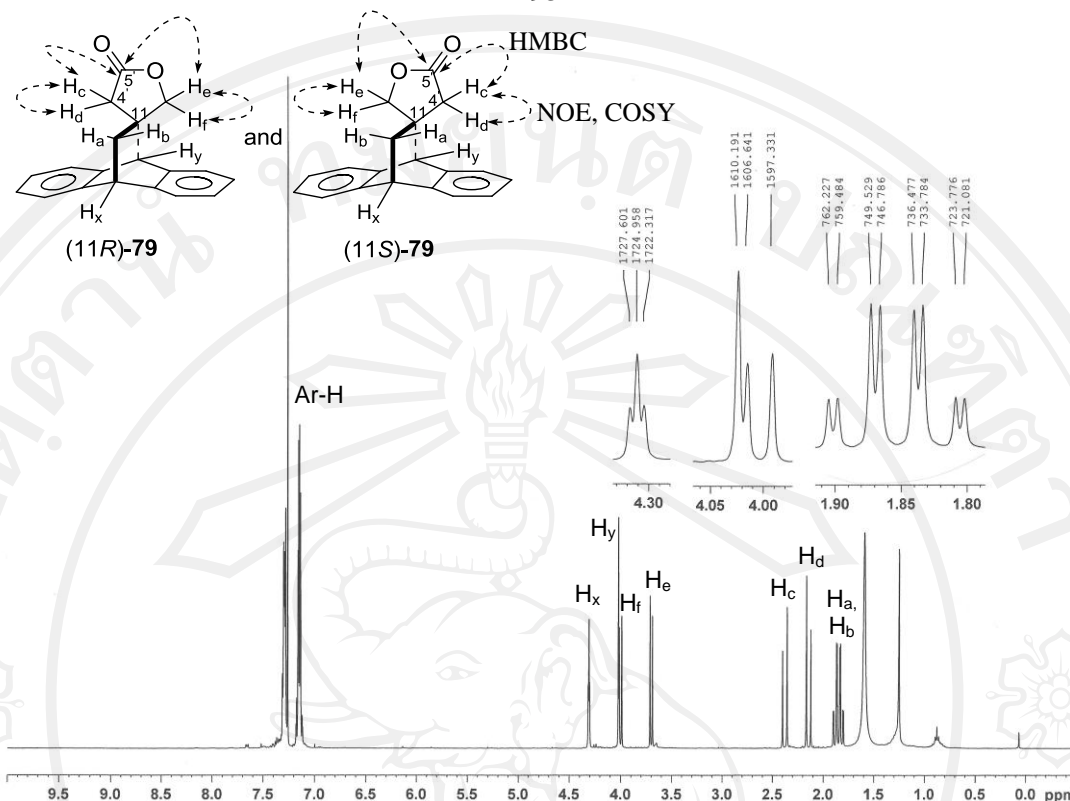


Figure 21 $^1\text{H-NMR}$ spectral data of by-products (11R)-**79** and (11S)-**79** (Dash arrows and plain arrows were COSY, NOE and HMBC correlation, respectively)

In case of by-product **80**, the signal of proton H_c and H_d appeared at 2.84 and 3.19 ppm as doublet ($J = 10.2$ Hz). Proton H_g and H_h showed at 3.51-3.56 ppm and 3.73-3.79 ppm as multiplet. Proton H_a , H_b , H_e and H_f showed at 1.23-1.43 ppm as multiplet. The correlation protons H_a , H_b , H_e and H_f and H_c , H_d and H_g , H_h were confirmed by COSY correlation. Furthermore, HMQC correlation showed that proton H_c and H_d correlated with methylene C-2', proton H_e and H_f correlated with methylene C-4' and proton H_g and H_h correlated with methylene C-5'. Besides, HMBC correlation illustrated that proton H_y ($\delta_{\text{H}} 4.33$, s) correlated with methylene C-2', proton H_c and H_d correlated with methylene C-4' and proton H_e and H_f correlated with methylene C-5' (Figure 22).

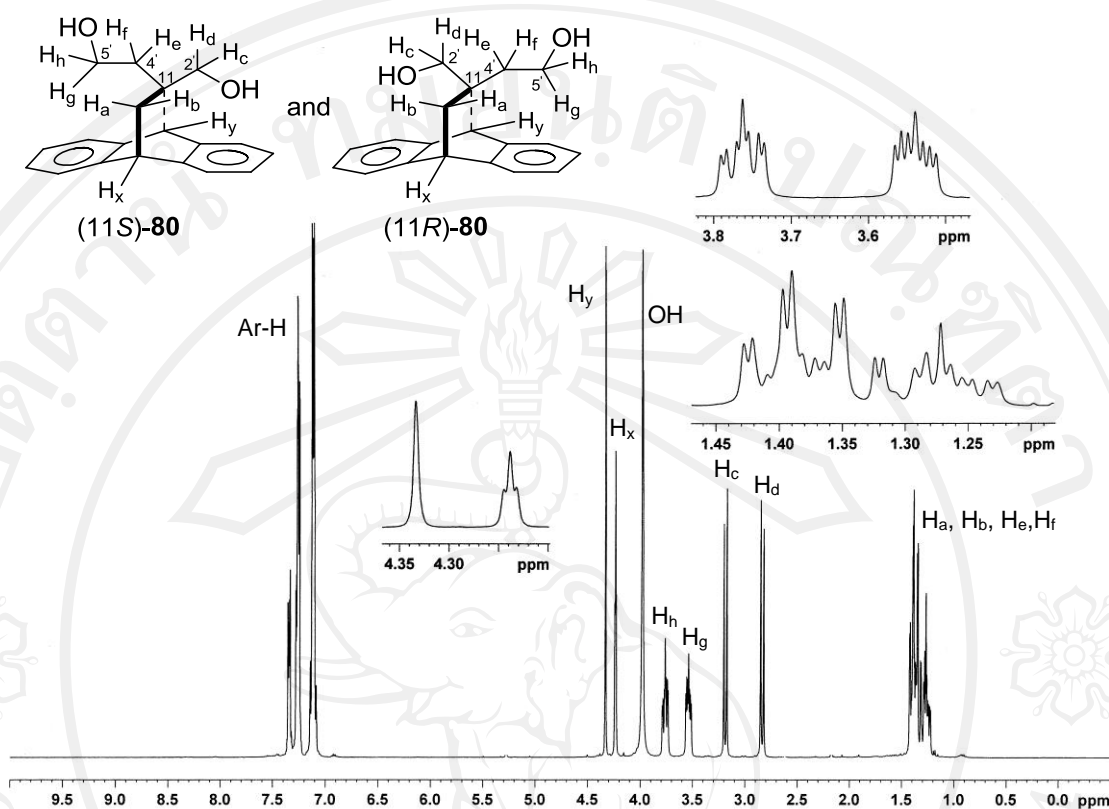


Figure 22 ^1H -NMR spectral data of by-products (11*S*)-**80** and (11*R*)-**80**

Table 29 depicted ^1H -NMR data of compounds (2'*S*,11*R*)-**70a** and (2'*R*,11*S*)-**70a**, (4'*R*,11*S*)-**78** and (4'*S*,11*R*)-**78**, (11*R*)-**79** and (11*S*)-**79** and (11*S*)-**80** and (11*R*)-**80**.

Table 29 $^1\text{H-NMR}$ data of TADDOL–anthracene adducts and by-products (2'*S*,11*R*)-**70a** and (2'*R*,11*S*)-**70a**, (4'*R*,11*S*)-**78** and (4'*S*,11*R*)-**78**, (11*R*)-**79** and (11*S*)-**79** and (11*S*)-**80** and (11*R*)-**80**

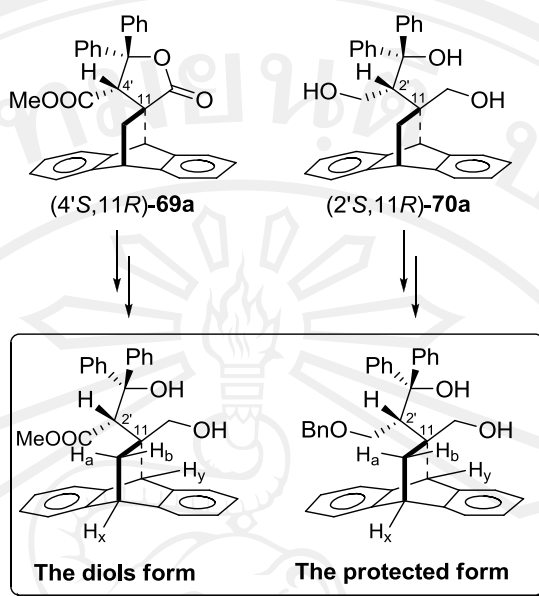
Compound	Physical property	m.p. (°C)	Chemical shift (δ , ppm)
(2' <i>S</i> ,11 <i>R</i>)- 70a and (2' <i>R</i> ,11 <i>S</i>)- 70a		202.7–204.2 and 184.0–187.0	0.52 1.36, 3.91 (<i>ABX</i> system ($J = 13.5$, 3.0, 2.6 Hz), 3H, H_a , H_b , H_x), 2.25 (<i>s</i> , 1H, H_c), 2.55, 4.25 (<i>d</i> , <i>AB</i> system ($J = 8.7$ Hz), 2H, CH_2 -2''), 2.60 (<i>s</i> , 1H, $-\text{OH}$ -1''), 3.97, 4.51 (<i>d</i> , <i>AB</i> system ($J = 12.9$ Hz), 2H, CH_2 -3'), 4.69 (<i>s</i> , 1H, H_y), 4.97 (<i>s</i> , 1H, $-\text{OH}$ -4'), 5.69 (<i>s</i> , 1H, $-\text{OH}$ -5'), 7.05-7.36 (<i>m</i> , 18H, ArH-1, 2, 3, 4, 5, 6, 7, 8, 2''', 3''', 4''', 5''', 6''', 2''''', 3''''', 4''''', 5''''', 6''''') (as shown in Figure 18)
(4' <i>R</i> ,11 <i>S</i>)- 78 and (4' <i>S</i> ,11 <i>R</i>)- 78	White crystals	195.9–196.5 and 197.0–198.6	1.16, 2.18, 4.02 (<i>ABX</i> system ($J = 13.4$, 3.0, 2.4 Hz), 3H, H_a , H_b , H_x), 3.01 (<i>s</i> , 1H, $-\text{OH}$), 3.41 (<i>s</i> , 1H, H_c), 3.67, 3.84 (<i>d</i> , <i>AB</i> system ($J = 8.7$ Hz), 2H, CH_2 -6'), 4.05 (<i>s</i> , 1H, H_y), 6.58-7.48 (<i>m</i> , 18H, ArH-1, 2, 3, 4, 5, 6, 7, 8, 2'', 3'', 4'', 5'', 6'', 2''', 3''', 4''', 5''', 6''') (as shown in Figure 20)
(11 <i>R</i>)- 79 and (11 <i>S</i>)- 79	White crystals	77.1–77.2 and 79.0–80.5	1.80-1.90, 4.31 (<i>ABX</i> system ($J = 12.7$, 2.7, 2.7 Hz), 3H, H_a , H_b , H_x), 2.15, 2.38 (<i>d</i> , <i>AB</i> system ($J = 17.4$ Hz), 2H, H_c , H_d), 3.70, 4.00 (<i>d</i> , <i>AB</i> system ($J = 9.3$ Hz), 2H, H_e , H_f), 2H), 4.02 (<i>s</i> , 1H, H_y), 7.13-7.31 (<i>m</i> , 8H, ArH-1, 2, 3, 4, 5, 6, 7, 8) (as shown in Figure 21)

Table 29 $^1\text{H-NMR}$ data of TADDOL–anthracene adducts and by-products (2'*S*,11*R*)-**70a** and (2'*R*,11*S*)-**70a**, (4'*R*,11*S*)-**78** and (4'*S*,11*R*)-**78**, (11*R*)-**79** and (11*S*)-**79** and (11*S*)-**80** and (11*R*)-**80** (continued)

Compound	Physical property	m.p. (°C)	Chemical shift (δ , ppm)
(11 <i>R</i>)- 80 and (11 <i>S</i>)- 80	White crystals	101.6–102.3 and 99.2–101.6	1.23-1.43 (<i>m</i> , 4H, H _a , H _b , H _c , H _f), 2.84, 3.19 (<i>d</i> , <i>AB</i> system ($J = 10.2$ Hz), 2H, H _c , H _d), 3.51-3.56 (<i>m</i> , 1H, H _g or H _h), 3.73-3.79 (H _h or H _g), 3.96 (<i>s</i> , 2H, alcohol), 4.23 (<i>s</i> , 1H, H _x), 4.33 (<i>s</i> , 1H, H _y), 7.07-7.36 (<i>m</i> , 8H, ArH-1, 2, 3, 4, 5, 6, 7, 8) (as shown in Figure 22)

3.4 Synthesis of optically active 11-hydroxymethylene-11-(2'-(1',3'-dihydroxy-1',1'-diphenylpropyl))-9,10-dihydro-9,10-ethanoanthracene derivatives [(2'*S*,11*R*)-**89** and (2'*S*,11*R*)-**90**]

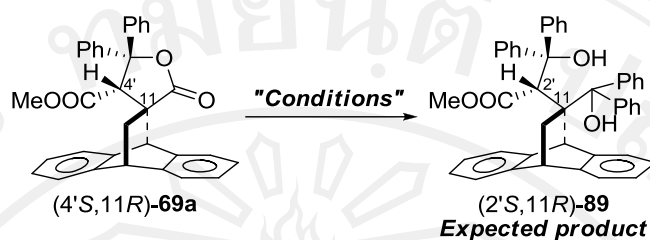
Importantly, synthesized TADDOL–anthracene catalyst in diols and protected forms [(2'*S*,11*R*)-**89** and (2'*S*,11*R*)-**90**] were investigated by various methods using major spiro–lactone adduct (4'*S*,11*R*)-**69a** and triol TADDOL–anthracene adduct (2'*S*,11*R*)-**70a** as model compounds, respectively (Scheme 18).



Scheme 18 The target TADDOL–anthracene catalysts in diols and protected forms.

3.4.1 Synthesis of 11-(1''-hydroxymethylphenyl)-11-([1'-hydroxy-diphenylmethyl]-methoxyacetyl)-9,10-dihydro-9,10-ethanoanthracene [(2'S,11R)-89]

Firstly, synthesized the diols form [(2'S,11R)-89] by using the major spiro–lactone adduct (4'S,11R)-69a with an excess of phenyl lithium (10 equiv) in the additives which were TMEDA and HMPA was studied. In these studies, the reactions were recovered starting material (entry 1 and 2, Table 30). Thus, we moved to study the synthesis of diols adduct by using PhMgBr as nucleophile under refluxing condition (entry 3, Table 30). It was found that the reaction gave the complex mixtures.

Table 30 Synthesis of TADDOL–anthracene adduct in the diols form

Entry	Conditions	Yield ^a (%)	Conversion (%)
1	i) 15.0 equiv PhBr, 10.0 equiv <i>n</i> -BuLi, 0°C, 1 hr. ii) 10.0 equiv PhLi, 10.0 equiv TMEDA –78°C to rt, overnight	Recovered (4' <i>S</i> ,11 <i>R</i>)- 69a	
2	i) 15.0 equiv PhBr, 10.0 equiv <i>n</i> -BuLi, 0°C, 1 hr. ii) 10.0 equiv PhLi, 10.0 equiv HMPA –78°C to rt, overnight	Recovered (4' <i>S</i> ,11 <i>R</i>)- 69a	
3	i) 5.0 equiv PhBr, 5.2 equiv Mg, reflux, 30 min ii) 10.0 equiv PhMgBr, reflux, 2 days	Complex mixtures	

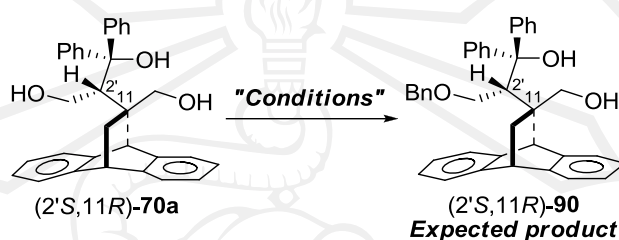
Due to the failure of synthesis the TADDOL–anthracene adduct in the diols form, we are interested in synthesizing the protected triol TADDOL–anthracene adduct as described in following section.

3.4.2 Protection of 11-hydroxymethylene-11-(2'-(1',3'-dihydroxy-1',1'-diphenylpropyl))-9,10-dihydro-9,10-ethanoanthracene [(2'*S*,11*R*)-**90**]

Next, investigation of synthesizing the protected TADDOL–anthracene adduct had been studied using triol TADDOL–anthracene adduct (2'*S*,11*R*)-**70a** as starting material. The triol TADDOL–anthracene adduct (2'*S*,11*R*)-**70a** was protected by benzyl bromide (1.3 equiv) using NaH (1.3 equiv) as base and THF or DMF as solvent stirred at 0°C to room temperature for overnight followed by 10%

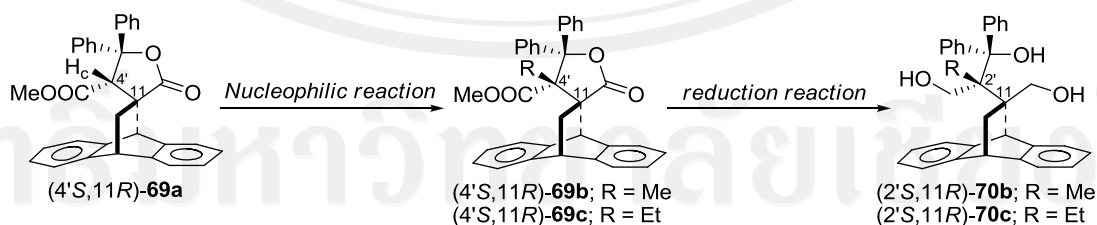
hydrochloric solution. Purification by flash column chromatography and preparative thin layer chromatography on silica gel with elution of EtOAc : hexane = 1 : 9 gave the complex mixtures. The results were shown in Table 31.

Table 31 Synthesis of the TADDOL–anthracene adduct in the protected form



Entry	Conditions	Yield ^a (%)	Conversion (%)
1	i) 1.3 equiv NaH/THF, 0°C ii) 1.3 equiv BnBr, 0°C to rt, overnight		Complex mixtures
2	i) 1.3 equiv NaH/DMF, 0°C ii) 1.3 equiv BnBr, 0°C to rt, overnight		Complex mixtures

From an unsuccessful of synthesizing TADDOL–anthracene adduct in the diols and protected forms (**89** and **90**), therefore, we are interested in synthesizing derivatives of TADDOL–anthracene adduct from spiro–lactone adduct (**4'S**)-(11*R*)-**69a** by substituted H_c with methyl and ethyl groups, respectively (Scheme 19).

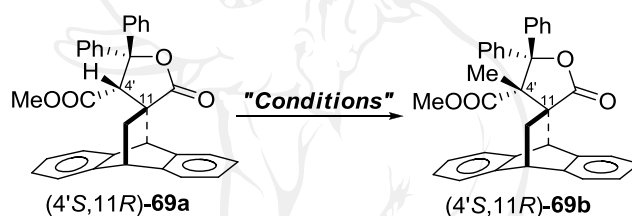


Scheme 19 Synthesis of TADDOL–anthracene adduct derivatives **70b** and **70c**.

3.5 Synthesis of enantiomeric of tetrahydro-4'-alkylcarbomethoxy-5'-diphenyl-2'-furanone-3'-spiro-11-9,10-dihydro-9,10-ethanoanthracenes [(4'*S*,11*R*)-**69b** and (4'*S*,11*R*)-**69b**]

Synthesized the spiro-lactone derivatives (**69b** and **69c**) was studied by varying the stoichiometric equivalent of lithium diisopropylamide (LDA) and addition of HMPA as cosolvent. Firstly, methyl spiro-lactone (4'*S*,11*R*)-**69b** was used as model reaction (Table 32).

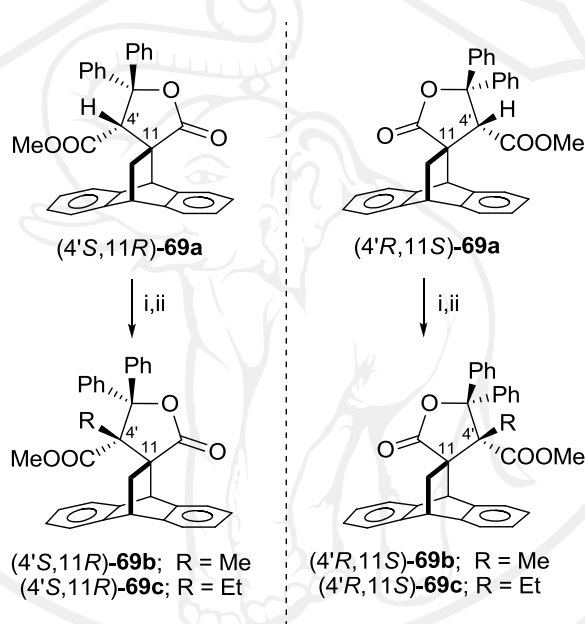
Table 32 Optimization of synthesizing methyl spiro-lactone (4'*S*,11*R*)-**69b**



Entry	Conditions	Yield ^a (%)	Conversion (%)
1	i) 1.2 equiv LDA/THF, -78°C, 1 hr. ii) 10.0 equiv MeI, -78°C to rt, overnight	Recovered (4' <i>S</i> ,11 <i>R</i>)- 69a	
2	i) 1.3 equiv LDA/THF, -78°C, 1 hr. ii) 10.0 equiv MeI, -78°C to rt, overnight	Recovered (4' <i>S</i> ,11 <i>R</i>)- 69a	
3	i) 2.0 equiv LDA/THF, -78°C, 1 hr. ii) 10.0 equiv MeI, -78°C to rt, overnight	Recovered (4' <i>S</i> ,11 <i>R</i>)- 69a	
4	i) 2.5 equiv LDA/THF, -78°C, 1 hr. ii) 10.0 equiv MeI, -78°C to rt, overnight	Recovered (4' <i>S</i> ,11 <i>R</i>)- 69a	
5	i) 3.0 equiv LDA/THF, -78°C, 1 hr. ii) 10.0 equiv MeI, -78°C to rt, overnight	Recovered (4' <i>S</i> ,11 <i>R</i>)- 69a	
6	i) 3.0 equiv LDA/THF, -78°C, 1 hr. ii) 3.0 equiv HMPA, -78°C, 2 hr. iii) 10.0 equiv MeI, -78°C to rt, overnight	31 ^a	99

^a Isolated yield

From Table 32, entry 1-5 without HMPA as additive showed the unreacted of spiro-lactone with methyl iodide. Hence, the effect of cosolvent which was HMPA in this reaction (entry 6) was studied. The reaction with an additive was successfully afforded methyl spiro-lactone (4'S,11R)-**69b** as product. Consequently, synthesis of the other optically active form and substitution by ethyl bromide were synthesized *via* this condition (Scheme 20).

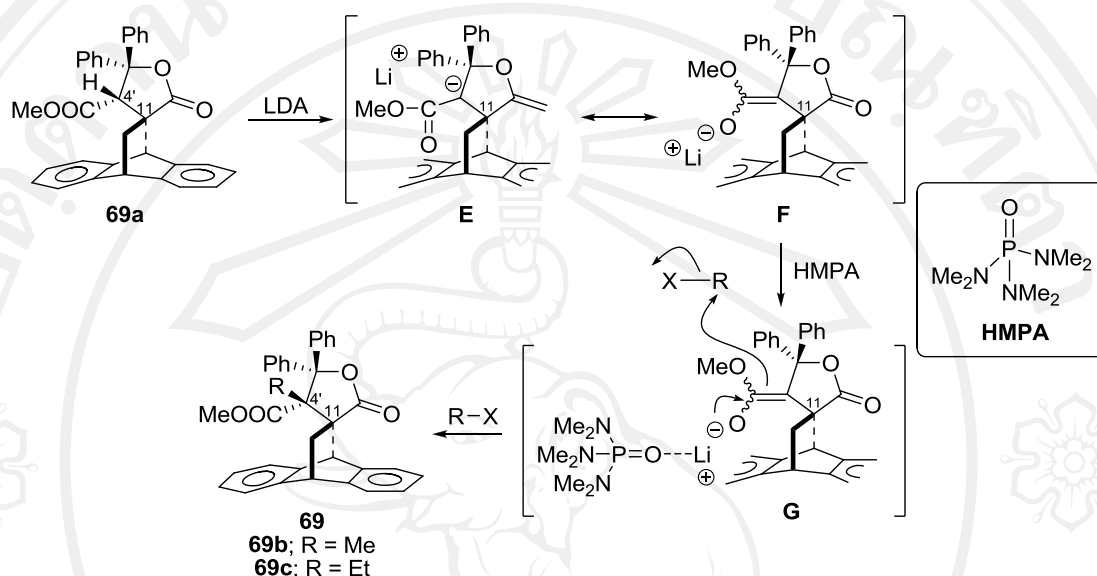


Scheme 20 Synthesis both of enantiomeric spiro-lactone derivatives **69b** and **69c**

Reagents and conditions: (i) a. 3.0 equiv LDA, THF, -78°C to 0°C , 1 h
 (ii) 3.0 equiv HMPA, -78°C (iii) 10.0 equiv MeI or 3.0 equiv EtBr, -78°C to rt, overnight.

The mechanism of this reaction could be explained. The enolate anions (**E** and **F**) were generated by spiro-lactone adduct (**69a**) reacted with 3.0 equiv LDA. Afterward, the lithium ion of intermediate **G** was strongly chelated with oxygen atom

of HMPA. Then, the intermediate **G** was reacted with alkyl halides which were methyl iodide or ethyl bromide as following Scheme 21.



Scheme 21 Proposed mechanism of synthesis spiro-lactone derivatives **69b** and **69c**.

The structures of methyl and ethyl spiro-lactone adducts were elucidated by ^1H NMR (Figure 24, 21 and Table 33) and NOE correlation.

Methyl spiro-lactone adducts ($4'R,11S$)-**69b** and ($4'S,11R$)-**69b**, the signal of methoxy proton-7' appeared at 3.17 ppm as singlet and methyl proton-8' at 2.97 ppm as doublet. Indeed, the position of methoxy proton-7' had shielding effect less than methyl proton-8' because of the electron withdrawing group of carbonyl group-6' as shown in Figure 24. The orientation of methyl group-8' was confirmed by NOE experiment. NOE correlation did not show the interaction between H_y and methyl-8'.

Thus, the orientation of methyl group-8' should be on the upper face as the same configuration. Furthermore, the structures of both enantiomeric methyl spiro-lactone adducts were confirmed by MM2 force field calculations for energy minimization from modeling program ChemBio3D Ultra 11.0 program as illustrated in Figure 23.

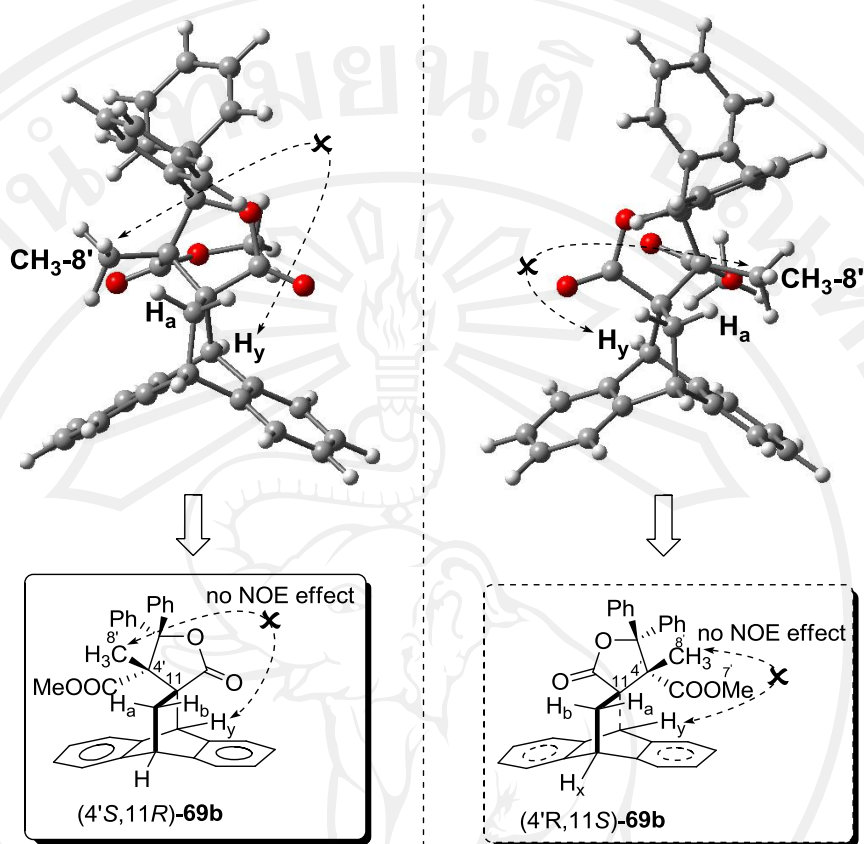


Figure 23 3D structural conformations of methyl spiro-lactone adducts (4'*R*,11*S*)-**69b** and (4'*S*,11*R*)-**69b** were generated by MM2 force field calculations for energy minimization from modeling program Chem3D Ultra 11.0 and GaussView 3.09 program with the observed NOE correlations (arrows)

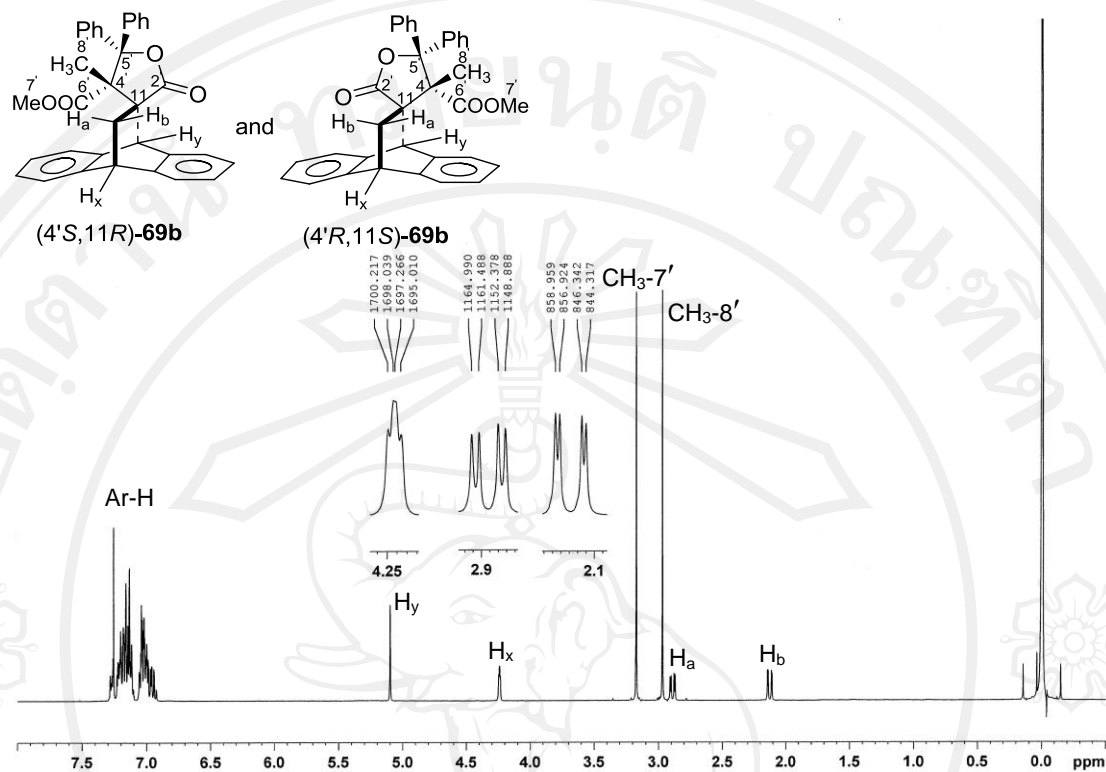


Figure 24 $^1\text{H-NMR}$ spectral data of methyl spiro-lactone adducts $(4'S,11R)$ -**69b** and $(4'R,11S)$ -**69b**

Considering ethyl spiro-lactone adducts $(4'R,11S)$ -**69c** and $(4'S,11R)$ -**69c**, methyl proton-9' showed signal at 0.99 ppm as triplet ($J = 7.5$ Hz), methoxy proton-7' at 2.99 ppm as singlet and methylene proton-8' at 3.41-3.53 ppm as multiplet. The orientation of ethyl group was confirmed by NOE experiment. Due to no interaction between H_y and ethyl group in NOE correlation, it demonstrated that the ethyl group should be on the upper face as the same configuration. Additionally, the structures of both enantiomeric ethyl spiro-lactone adducts were confirmed by MM2 force field calculations for energy minimization from modeling program ChemBio3D Ultra 11.0 program as illustrated in Figure 25.

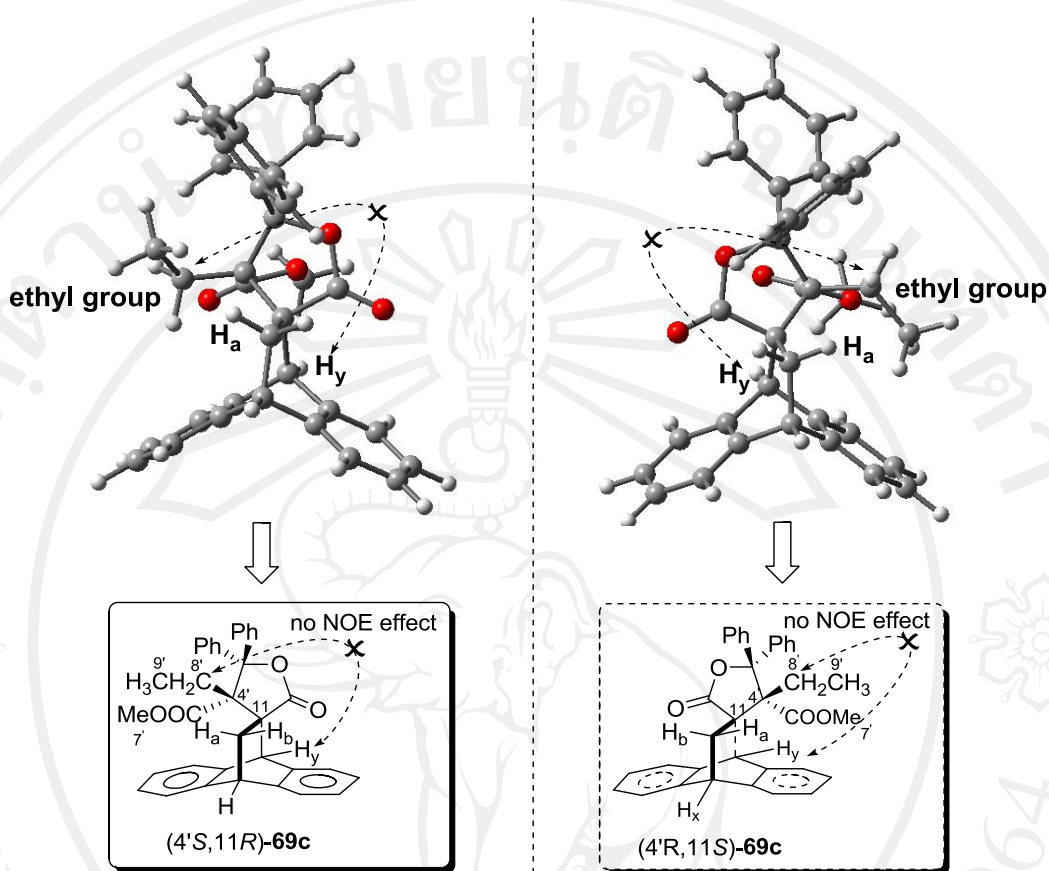


Figure 25 3D structural conformations of ethyl spiro-lactone adducts (4'*R*,11*S*)-**69c** and (4'*S*,11*R*)-**69c** were generated by MM2 force field calculations for energy minimization from modeling program Chem3D Ultra 11.0 and GaussView 3.09 program with the observed NOE correlations (arrows)

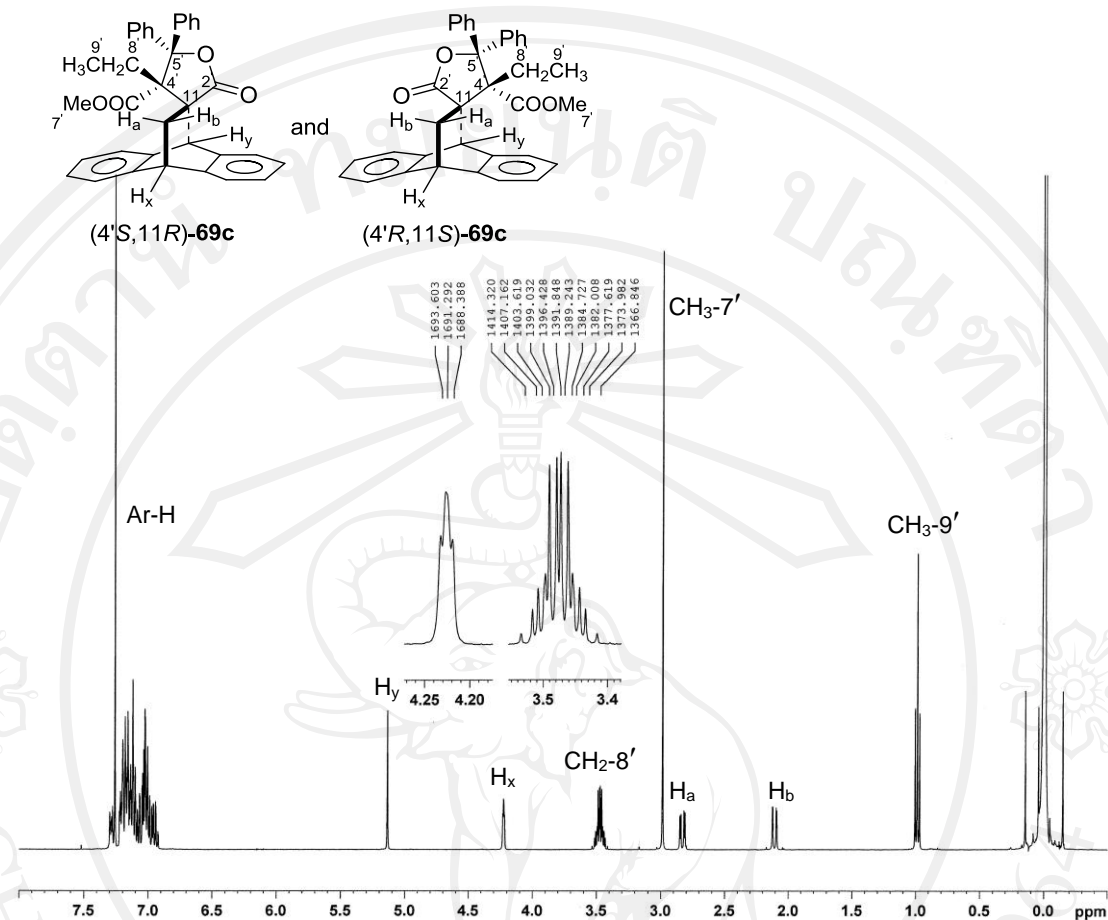


Figure 26 $^1\text{H-NMR}$ spectral data of ethyl spiro-lactone adducts (4'*S*,11*R*)-**69c** and (4'*R*,11*S*)-**69c**

Table 33 depicted $^1\text{H-NMR}$ data of optically active spiro-lactone derivatives (**69b** and **69c**).

Table 33 $^1\text{H-NMR}$ data of optically active spiro-lactone derivatives (**69b** and **69c**)

Compound	Physical property	m.p. (°C)	Chemical shift (δ , ppm)
(4' <i>S</i> ,11 <i>R</i>)- 69b and (4' <i>R</i> ,11 <i>S</i>)- 69b	White crystals	199.5–200.9 and 198.0–201.0	2.13, 2.89, 4.24 (<i>ABX</i> system ($J = 12.6, 3.5, 2.2$ Hz), 3H, H_a, H_b, H_x), 2.97 (<i>s</i> , 3H, $\text{CH}_3\text{-8}'$), 3.17 (<i>s</i> , 3H, $\text{COOCH}_3\text{-7}'$), 3.42 (<i>s</i> , 1H, H_c), 5.10 (<i>s</i> , 1H, H_y), 6.92-7.29 (<i>m</i> , 18H, ArH) (<i>m</i> , 18H, ArH-1, 2, 3, 4, 5, 6,

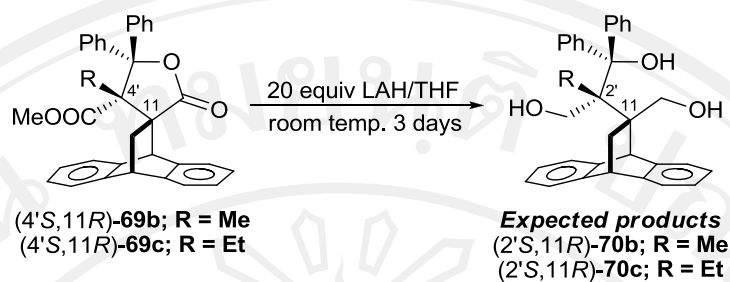
Table 33 $^1\text{H-NMR}$ data of optically active spiro–lactone derivatives (**69b** and **69c**)

(continued)

Compound	Physical property	m.p. (°C)	Chemical shift (δ , ppm)
			7, 8, 2', 3', 4', 5', 6', 2'', 3'', 4'', 5'', 6'') (as shown in Figure 24)
(4' <i>S</i> ,11 <i>R</i>)- 69c and (4' <i>R</i> ,11 <i>S</i>)- 69c	White powder	185.4–186.8 and 186.1–187.8	0.99 (<i>t</i> , $J = 7.5$ Hz, 3H, CH_3 -9'), 2.11, 2.83, 4.23 (<i>ABX</i> system ($J = 12.7, 3.5, 2.3$ Hz), 3H, $\text{H}_a, \text{H}_b, \text{H}_x$), 2.99 (<i>s</i> , 3H, CH_3 -7'), 3.41-3.53 (<i>m</i> , 2H, CH_2 -8'), 5.14 (<i>s</i> , 1H, H_y), 6.94-7.30 (<i>m</i> , 18H, Ar-H-1, 2, 3, 4, 5, 6, 7, 8, 2', 3', 4', 5', 6', 2'', 3'', 4'', 5'', 6'') (as shown in Figure 26)

3.6 Reduction of tetrahydro-4'-alkylcarbomethoxy-5'-diphenyl-2'-furanone-3'-spiro-11-9,10-dihydro-9,10-ethanoanthracenes [(2'*S*,11*R*)-**69b** and (2'*S*,11*R*)-**69c**]

The next study, we focused on the triol TADDOL–anthracene adduct derivatives (2'*S*,11*R*)-**70b** and (2'*S*,11*R*)-**70c** by reducing the spiro–lactone derivatives, methyl and ethyl spiro–lactones (**69b** and **69c**), with an excess LAH (20 equiv) in THF for 3 days. Quenched with acetone then passed through Celite 545 and purified by flash column chromatography on silica gel with elution EtOAc : hexane = 1 : 9. It was found that the reactions gave the complex mixture as products (Scheme 22).



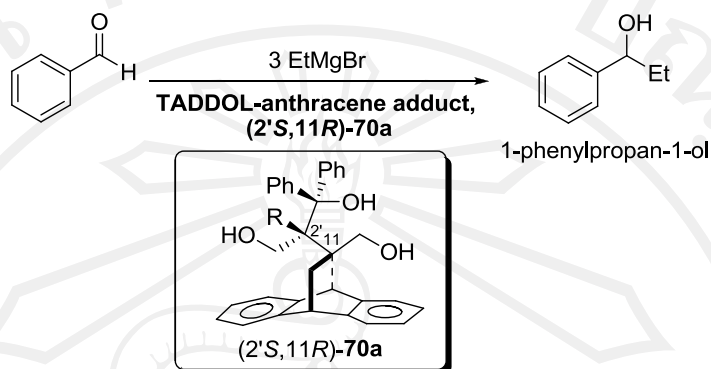
Scheme 22 Reduction of methyl and ethyl spiro-lactone adducts by an excess LAH.

The reductions of spiro-lactone derivatives (**69b** and **69c**) were unsuccessfully due to obtain the mixture complexes. Consequently, the triol TADDOL-anthracene adducts (2'S,11R)-**70a** and (2'R,11S)-**70a** were studied as catalysts in 1,2-addition of ethyl magnesium bromide to benzaldehyde and reduction the β -keto ester by NaBH_4 .

3.7 Study the effect of the triol TADDOL-anthracene catalysts for 1,2-addition reaction of ethyl magnesium bromide to benzaldehyde

The 1,2-addition reaction of ethyl magnesium bromide to benzaldehyde was studied by using the triol TADDOL-anthracene adduct (2'S,11R)-**70a** as model compound (Table 34).

Table 34 Effect of the triol TADDOL–anthracene adduct (2'*S*,11*R*)-**70a** in 1,2-addition



Entry	Conditions	Yield (%) ^a	Conversion (%)	Configuration of product ^b
1	i) 3 mol EtBr, Mg turning, reflux 30 min ii) benzaldehyde, 0°C, 1 hr.	41	100	-
2	i) 3 mol EtBr, Mg turning, reflux 30 min ii) 1 mol% [(2' <i>S</i> ,11 <i>R</i>)- 70a], 0°C, 15 min iii) benzaldehyde, 0°C, 1.30 hr.	54	100	<i>R</i>
3	i) 3 mol EtBr, Mg turning, reflux 30 min ii) 1.4 mol Ti(<i>i</i> OPr) ₄ , benzaldehyde, 0°C iii) 1 mol% [(2' <i>S</i> ,11 <i>R</i>)- 70a], 0°C, 1 hr. iv) benzaldehyde, 0°C, 1.30 hr.	complex mixtures		-

^a Isolated yield

^b Configuration of product was determined by the sign of specific rotation compared with the literature, $[\alpha]_D^{27.0} = +286.85^\circ$ ($c = 0.502$, CHCl₃) [lit²⁰: $[\alpha]_D^{27.0} = +17.5^\circ$ ($c = 0.860$, CHCl₃).

As can be seen from Table 34, there were no significant in terms of increasing percent yield of 1-phenylpropan-1-ol when TADDOL–anthracene adduct (2'*S*,11*R*)-**70a** was used (entry 1 and 2). Correspondingly, addition of Ti(*i*OPr)₄ together with (2'*S*,11*R*)-**70a** influenced to give complex mixture as products (entry 3).

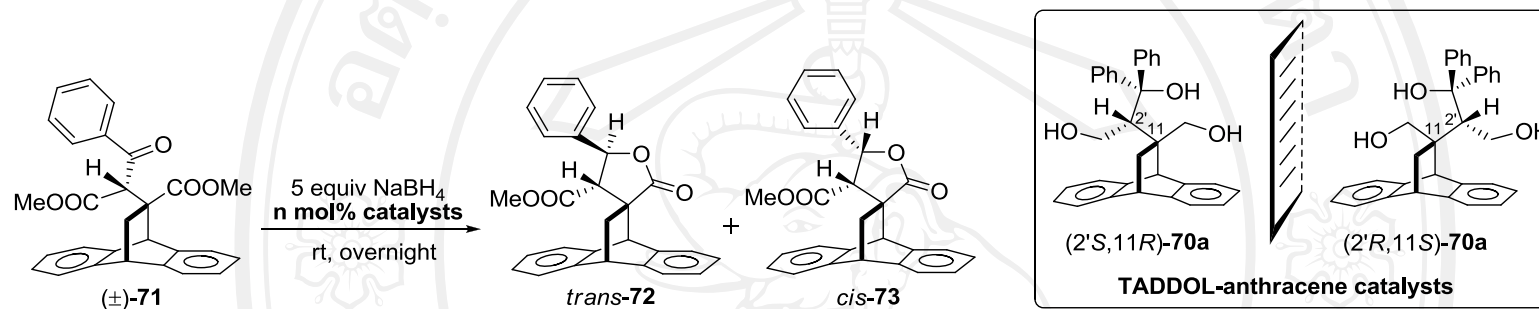
Owning to the failure of using TADDOL–anthracene adduct (2'*S*,11*R*)-**70a** to catalyze the 1,2-addition reaction, we therefore investigated the effect of

TADDOL–anthracene adducts (2'S,11R)-**70a** and (2'R,11S)-**70a** in reduction reaction as following topic.

3.8 Study the effect of the triol TADDOL–anthracene catalysts for reduction reaction of 11-carbomethoxy-11-(1'-benzoyl)methoxyacetyl-9,10-dihydro-9,10- ethanoanthracene [(±)-71]

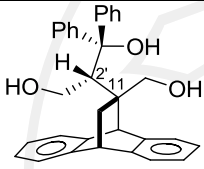
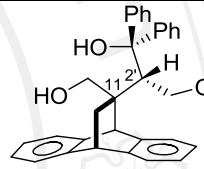
Reduction of β -keto ester (±)-**71** by NaBH₄ in the presence of the triol TADDOL–anthracene adducts (2'S,11R)-**70a** and (2'R,11S)-**70a** as catalysts was investigated by various concentration the catalysts as shown in Table 35.

Table 35 Reduction of β -keto ester (\pm)-**71** by NaBH₄ in the presence of (2'*S*,11*R*)-**70a** and (2'*R*,11*S*)-**70a**



Entry	n mol% of catalysts	Catalysts									
		(2' <i>S</i> ,11 <i>R</i>)- 70a					(2' <i>R</i> ,11 <i>S</i>)- 70a				
		% Yield ^a		Ratio		% Conversion	% Yield ^a		Ratio		% Conversion
		<i>trans</i> -isomer	<i>cis</i> -isomer	<i>trans</i> : <i>cis</i>			<i>trans</i> -isomer	<i>cis</i> -isomer	<i>trans</i> : <i>cis</i>		
1	1	32	15	2.17:1	68:32	99	40	2	20:1	95:5	100
2	1% THF:H ₂ O (4:0.5)	47	11	4.27:1	81:19	100	53	74	0.72:1	42:58	100
3	5	24	20	1.20:1	55:45	83	39	16	2.44:1	71:29	100

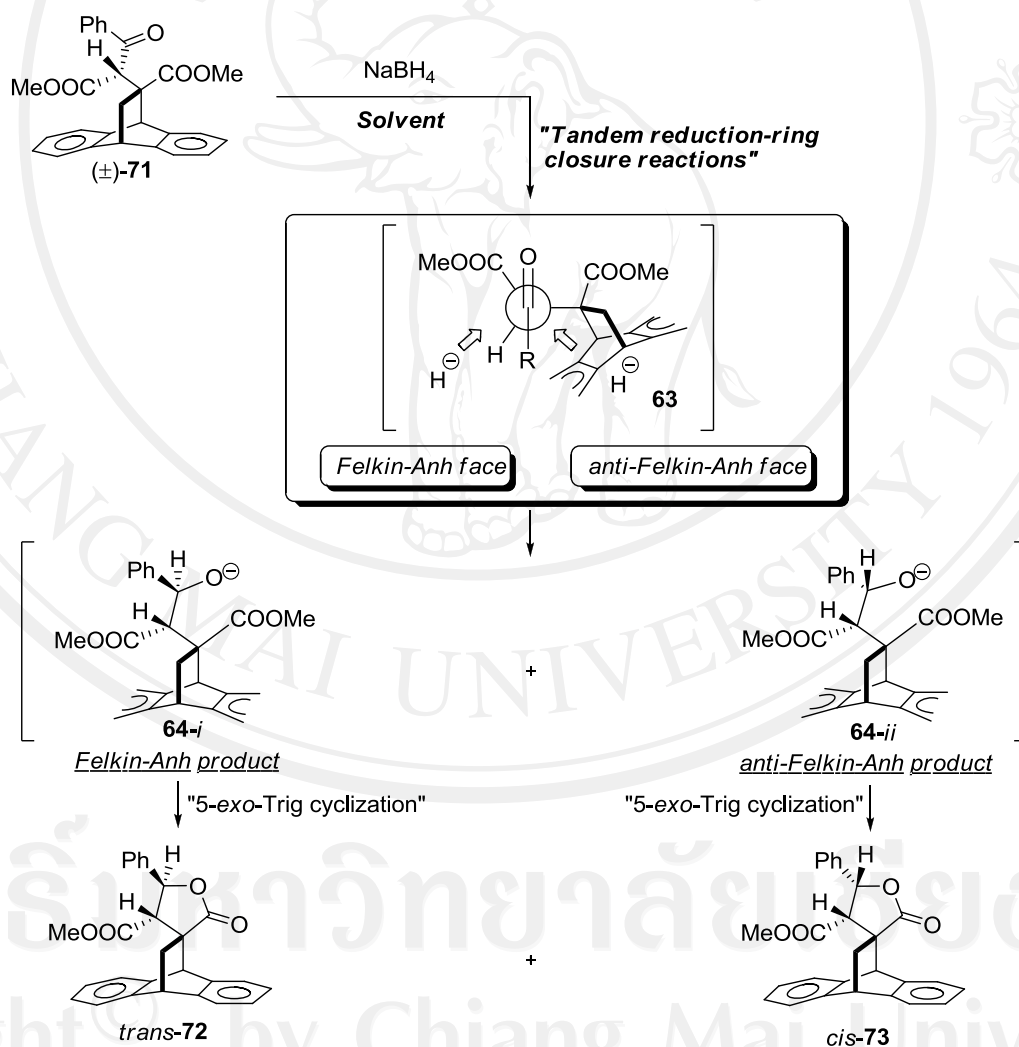
Table 35 Reduction of β -keto ester (\pm)-**71** by NaBH₄ in the presence of (2'*S*,11*R*)-**70a** and (2'*R*,11*S*)-**70a** (continued)

Entry	n mol% of catalysts	Catalysts									
		 (2' <i>S</i> ,11 <i>R</i>)- 70a					 (2' <i>R</i> ,11 <i>S</i>)- 70a				
		% Yield ^a		Ratio		% Conversion	% Yield ^a		Ratio		% Conversion
		<i>trans</i> -isomer	<i>cis</i> -isomer	<i>trans:cis</i>			<i>trans</i> -isomer	<i>cis</i> -isomer	<i>trans:cis</i>		
4	10	10	25	0.40:1	29:71	100	40	16	2.50:1	72:28	100
5	15	43	13	3.31:1	77:23	89	50	16	3.13:1	76:24	100
6	20	35	13	2.64:1	73:27	89	46	13	3.54:1	78:22	100

^a NMR yield

In the previous study, Jongkol and coworkers reported the reduction of β -keto ester adduct by NaBH_4 in THF : H_2O (4 : 0.5) system that obtained *trans*-72 and *cis*-73 in the highest diastereoselectivity, *trans*:*cis* = 97 : 3, and high yield (70% yield *trans*-isomer and 2% yield *cis*-isomer).²¹ Thus, applied the triol TADDOL–anthracene adducts (2'*S*,11*R*)-70a and (2'*R*,11*S*)-70a as catalysts was investigated.

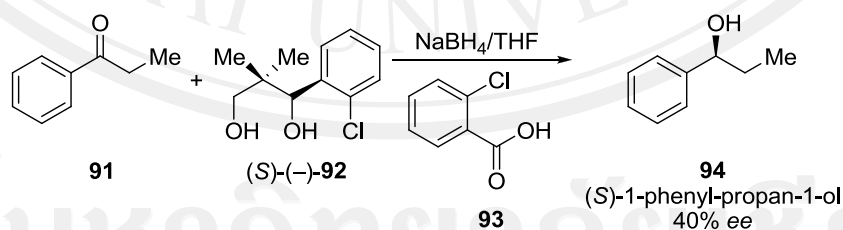
Jongkol *et al.* proposed the reduction mechanism using Felkin-Anh model to describe (Scheme 23).



Scheme 23 Proposed mechanism of β -keto ester reduction by Jongkol.^{21b}

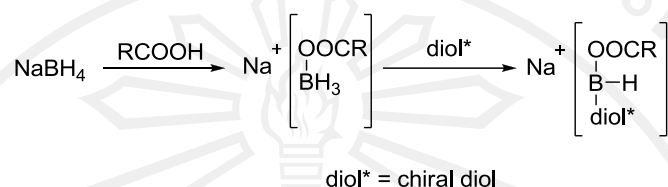
In case of catalyst [(2'*S*,11*R*)-**70a**], there were no influence in terms of increasing percent yield of *trans*- and *cis*-isomers when increasing mol% of catalyst was used. However, at 10 mol% of catalyst [(2'*S*,11*R*)-**70a**] caused to increase *cis*-isomer more than *trans*-isomer (entry 4). In addition, compound [(2'*R*,11*S*)-**70a**] as catalyst, the highest diastereoselectivity was performed by 1 mol% of catalyst in ratio of *trans*:*cis* = 95:5 (entry 1). It can be concluded that at 1 mol% of the triol TADDOL–anthracene adduct in form [(2'*R*,11*S*)-**70a**] provided the highest *trans*:*cis*-isomer selectivity.

Despite the reduction mechanism was not exactly clear, a proposed mechanism of reduction β -keto ester by NaBH₄ and the triol TADDOL–anthracene adducts (2'*S*,11*R*)-**70a** and (2'*R*,11*S*)-**70a** as catalysts was proposed according to Xianming, H. and Kellogg, R. M. studied.²² Xianming, H. *et al.* studied the asymmetric reduction of prochiral aromatic ketones by NaBH₄ modified with optically pure 1-aryl-2,2-dimethyl-1,3-propanediols and chlorobenzoic acid (**93**) in THF. Scheme 25 represents the reduction of propiophenone (**91**) in the presence of (*S*)-(-)-2,2-dimethyl-1-(2'-chlorophenyl)-1,3-propanediols (*S*)-(-)-**92** and chlorobenzoic acid (Scheme 24).



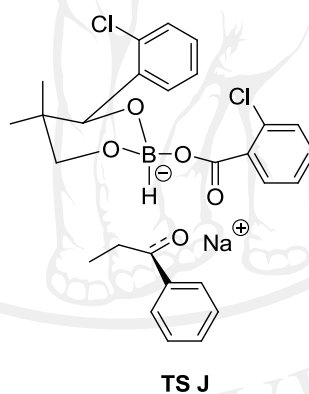
Scheme 24 The asymmetric reduction of prochiral aromatic ketones by chirally modified NaBH₄.²²

Xianming, H. *et al.* explained that the reaction of NaBH₄ with an acid and two free hydroxyl groups in the alcohol forms a reduction reagent, which contains active hydrogen surrounded by a bulky asymmetric structure (Scheme 25).



Scheme 25 Mechanism of NaBH₄ and carboxylic acid with chiral diols.²²

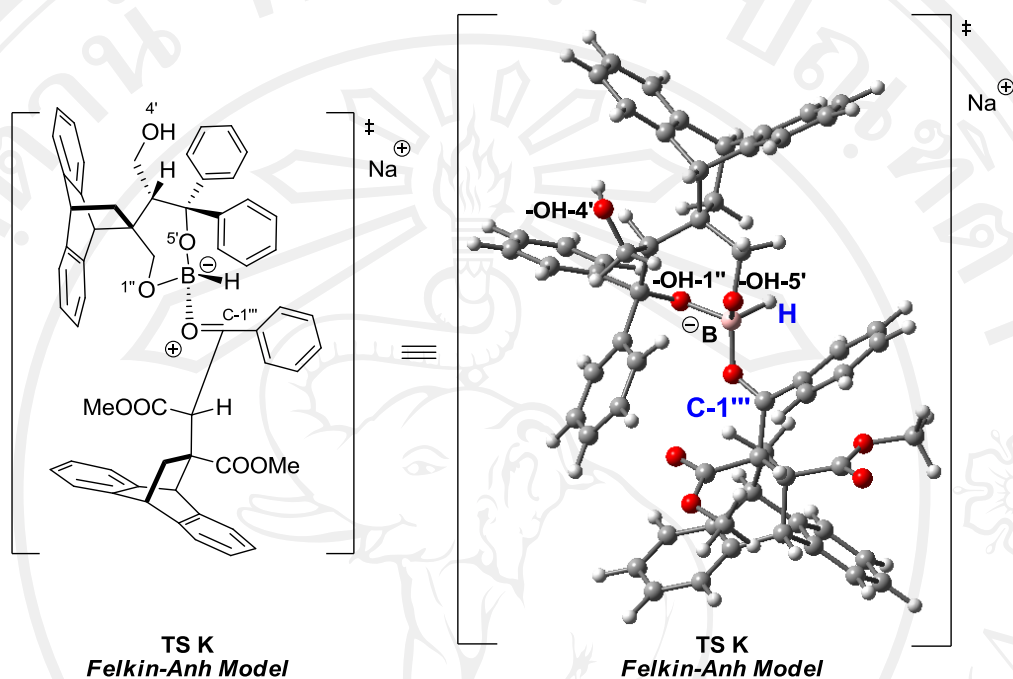
They suggested that the asymmetric reduction of propiophenone in the presence of compound (*S*)-(-)-**92** could be proposed through transition state model **J** as shown in Scheme 26.



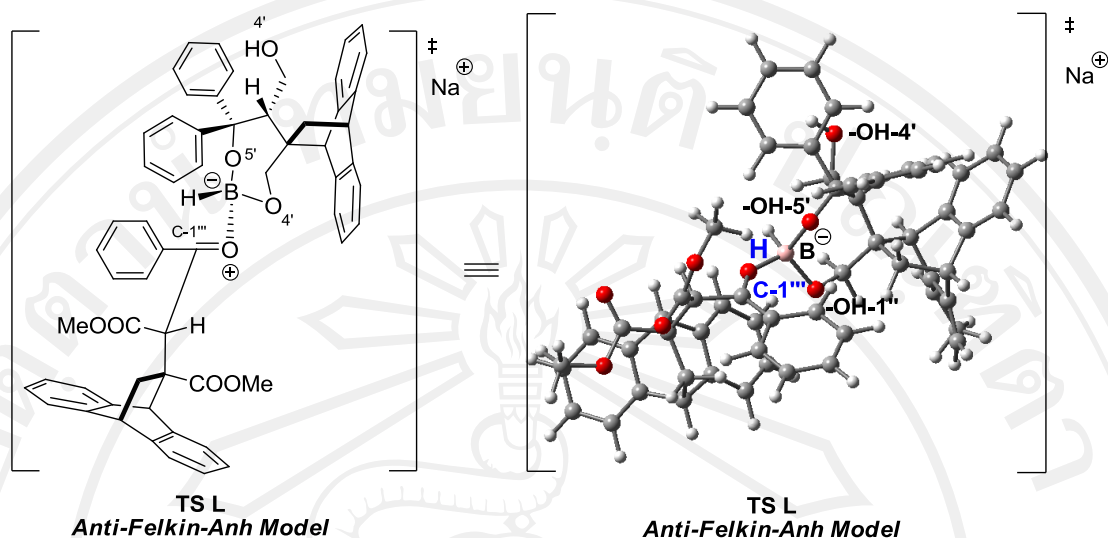
Scheme 26 Transition state model for reduction of propiophenone by chirally modified NaBH₄.

Based on Xianming, H. *et al.* model, the reduction mechanism in the presence of the triol TADDOL–anthracene adducts (*2'S,11R*)-**70a** and (*2'R,11S*)-**70a** as catalysts could be proposed. The 3D structural conformations of transition state models were generated by MM2 force field calculations for energy minimization from modeling program ChemBio 3D Ultra 11.0 and GaussView 3.09 program. In order to

propose the transition states of the triol TADDOL–anthracene adducts chelation with NaBH_4 , Felkin-Anh model was used to explain as shown below.

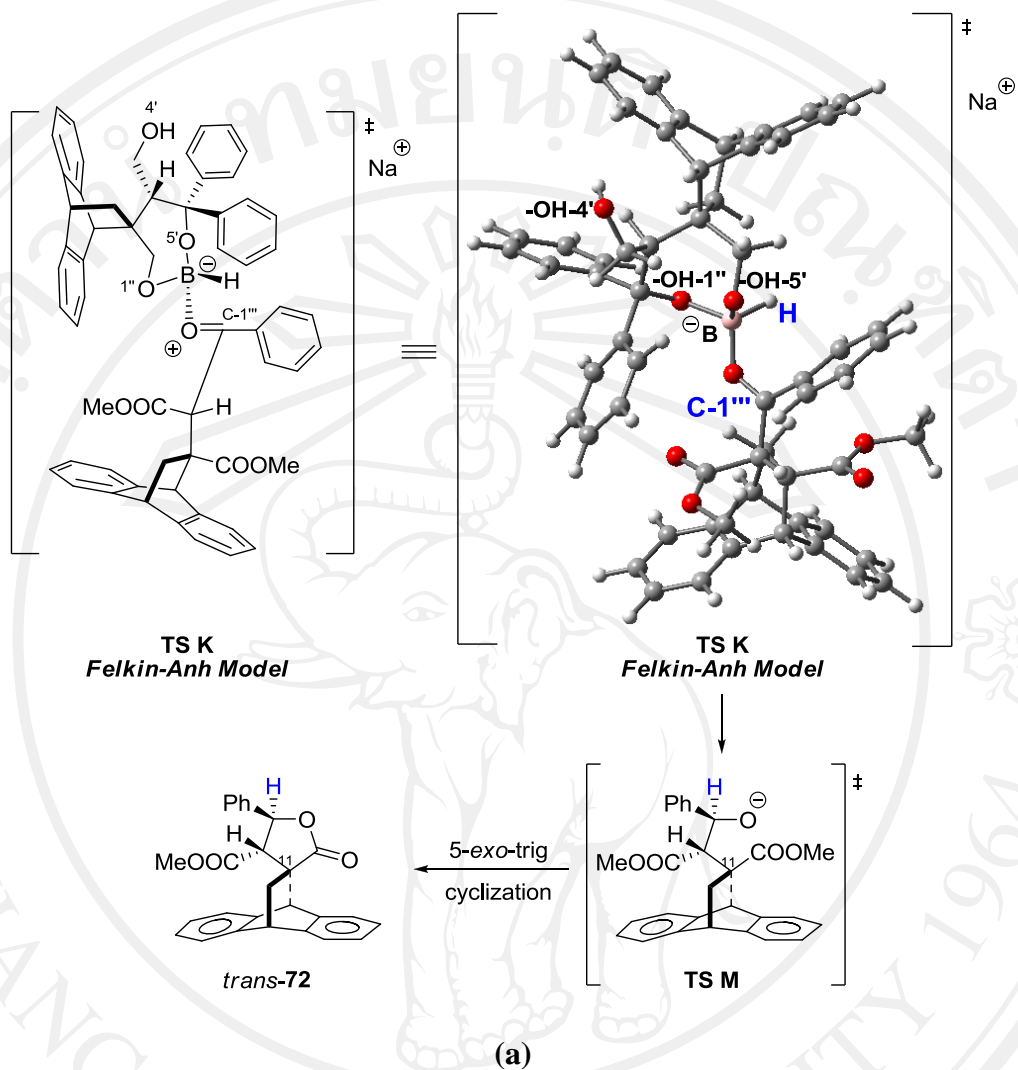


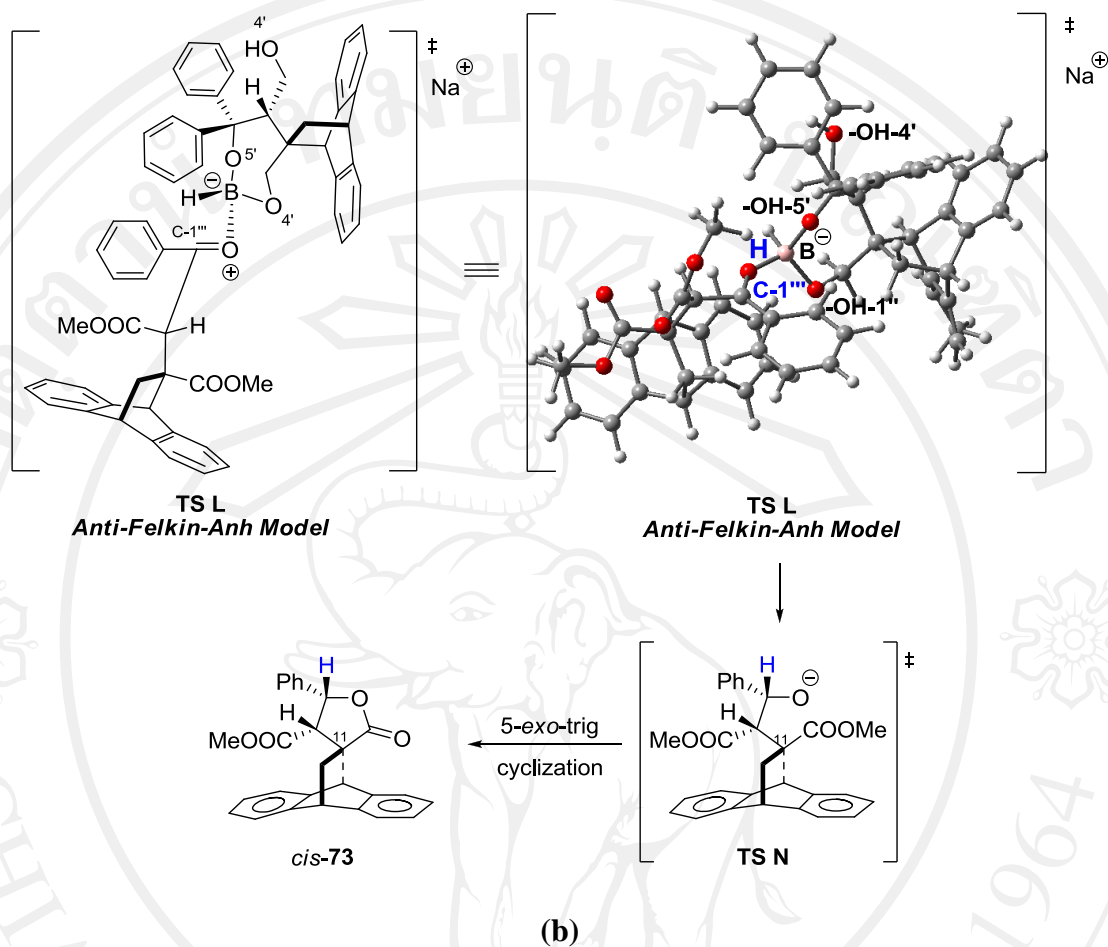
Scheme 27 Proposed transition state models for the triol TADDOL–anthracene adduct (2'S,11R)-70a via Felkin-Anh model.



Scheme 28 Proposed transition state models for the triol TADDOL–anthracene adduct (2'*S*,11*R*)-**70a** via Anti-Felkin-Anh model.

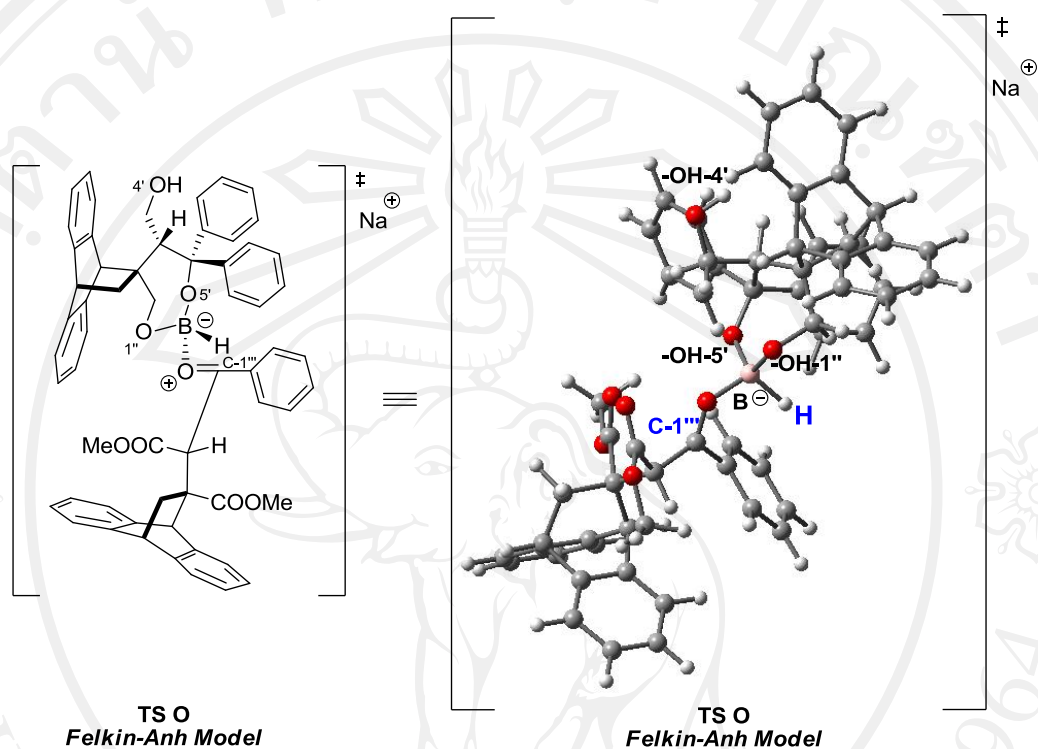
Considering the minimization energy of those two models above, TS **K** and TS **L**, TS **K** (Scheme 27) had the total energy 76.7854 kcal/mol. Comparatively, the total energy of TS **L** (Scheme 28) was 90.3224 kcal/mol. To examine the mechanism of this reaction, carbonyl-C-1''' was attacked by hydride from above. Hence, Felkin-Anh model (TS **K**) led to *trans*-isomer (Scheme 29a). On the other hand, *cis*-isomer was observed from Anti-Felkin-Anh model (Scheme 29b). Scheme 29a and 29b represents the mechanism of *trans*- and *cis*-isomers, respectively.



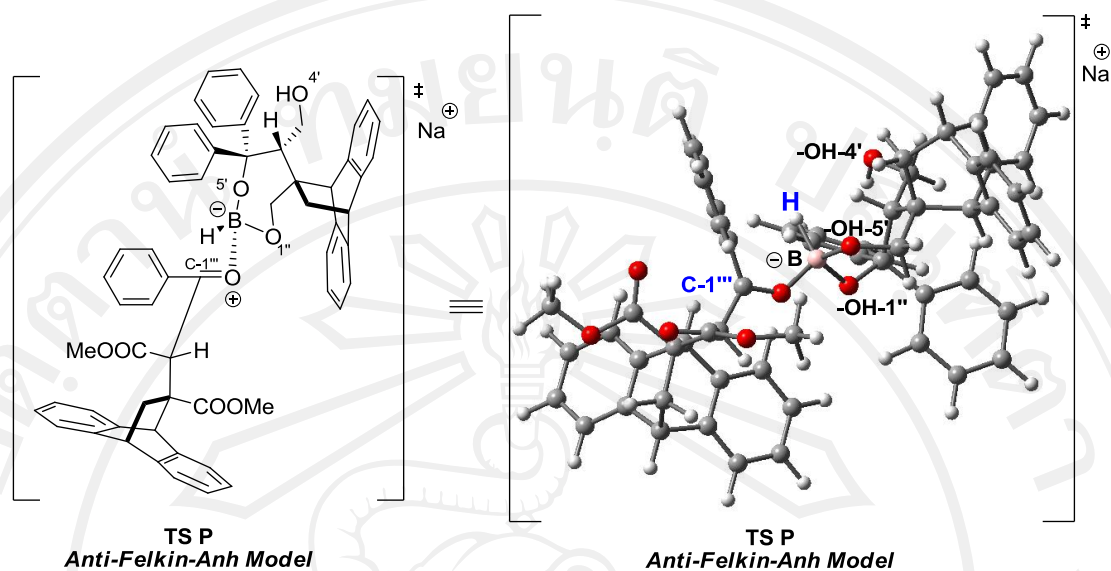


Scheme 29 Proposed mechanism for the triol TADDOL-anthracene adduct (2'S,11R)-70a. (a) Mechanism for *trans*-isomer. (b) Mechanism model for *cis*-isomer.

Accordingly, the transition state models of TADDOL–anthracene adducts (2'*R*,11*S*)-**70a** were proposed *via* Felkin-Anh model as shown in Scheme 30 and 31.

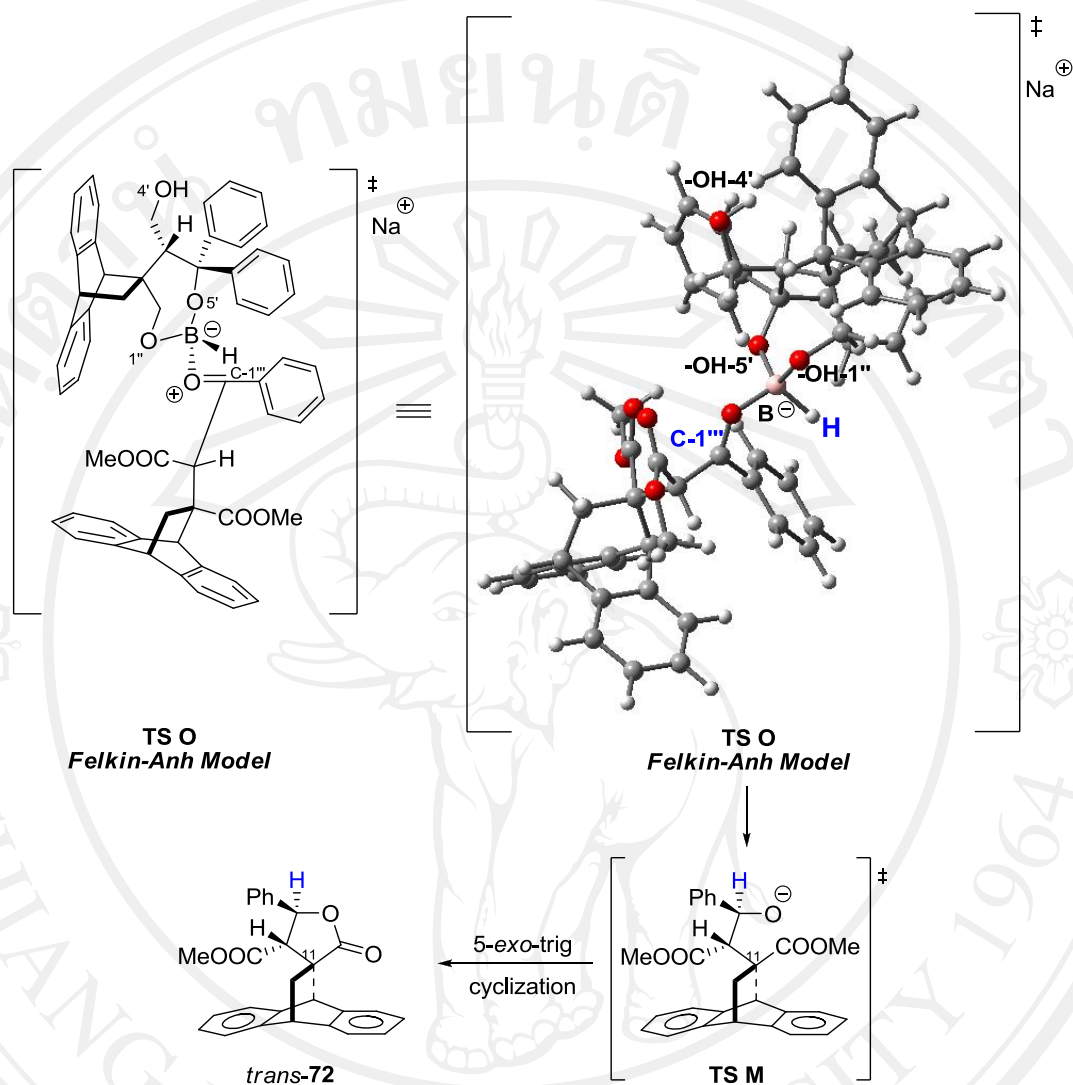


Scheme 30 Proposed transition state models for the triol TADDOL–anthracene adduct (2'*R*,11*S*)-**70a** *via* Felkin-anh model.

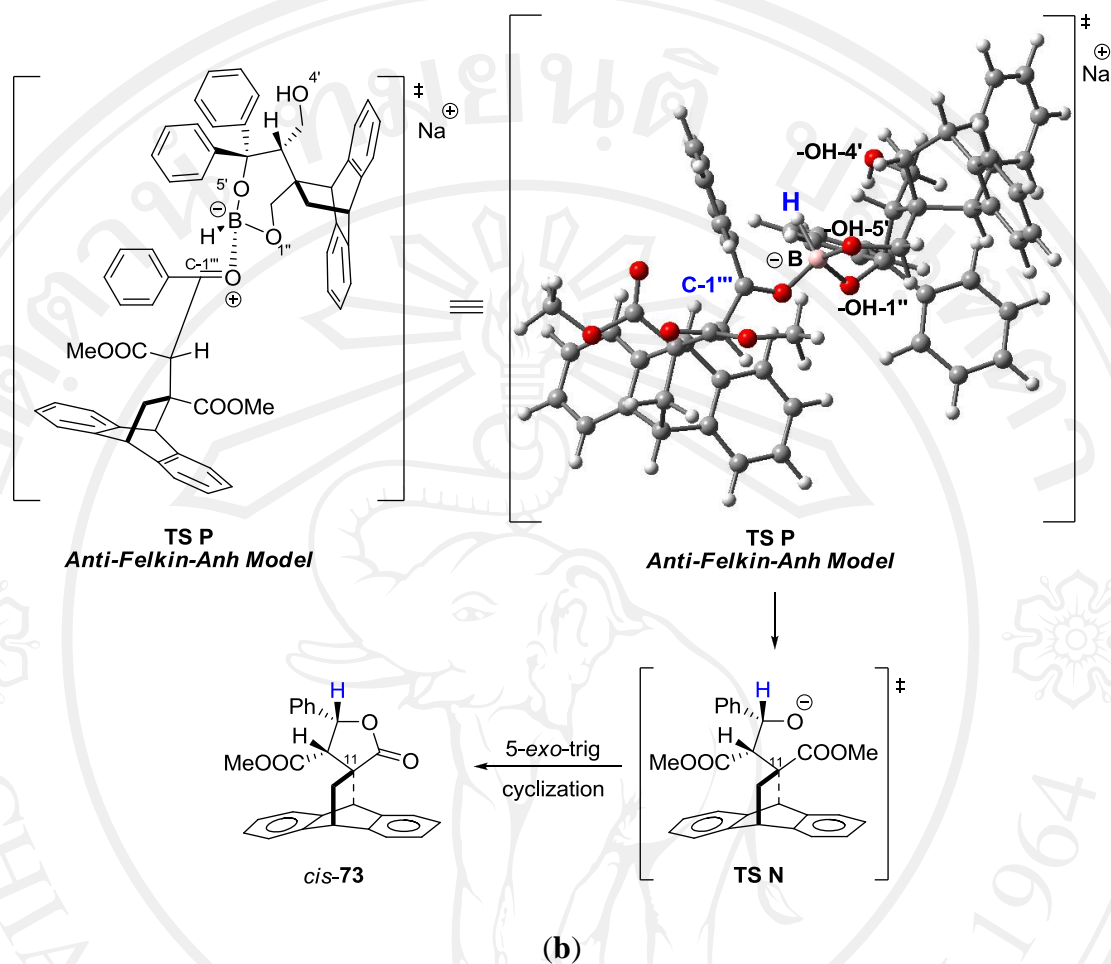


Scheme 31 Proposed transition state models for the triol TADDOL–anthracene adduct (2'*R*,11*S*)-**70a** via Anti-Felkin-anh model.

Similarly, the minimization energy of TS **O** and TS **P** were 81.1339 and 80.3562 kcal/mol, respectively. Besides, the ratio of *trans*:*cis*-isomer when used this catalyst was slightly different due to the minimization energy of those two models. However, it was complicated to explain why 1 mol% of catalyst [(2'*R*,11*S*)-**70a**] gave the highest diastereoselectivity (*trans*:*cis* = 95:5, entry 1, Table 35). The mechanism of *trans*- and *cis*-isomers was shown in Scheme 32a and 32b, respectively.



(a)



Scheme 32 Proposed mechanism for the triol TADDOL-anthracene adduct (2'*R*,11*S*)-70a. (a) Mechanism for *trans*-isomer. (b) Mechanism model for *cis*-isomer.